Low Temperature Physics

Knowns and unknowns in the Davydov model for energy transfer in proteins

Cite as: Low Temp. Phys. **48**, 973 (2022); https://doi.org/10.1063/10.0015107
Submitted: 24 October 2022 • Published Online: 07 December 2022

Leonor Cruzeiro

Low Temperature Physics ARTICLE scitation.org/journal/ltp

Knowns and unknowns in the Davydov model for energy transfer in proteins

Cite as: Fiz. Nizk. Temp. **48**, 1105–1126 (December 2022); doi: 10.1063/10.0015107
Submitted: 24 October 2022

Leonor Cruzeiro[1,a]

AFFILIATIONS

[1]CCMAR/CIMAR — Centro de Ciências do Mar and Physics, FCT, Universidade do Algarve, Campus de Gambelas, 8005-139 Faro, Portugal

[a)]**Author to whom correspondence should be addressed:** lhansson@ualg.pt

ABSTRACT

The Davydov model for amide I propagation in hydrogen-bonded chains of proteins is revisited. The many similarities between the mixed quantum-classical dynamical equations and those that are derived from the full quantum Davydov model while applying the so-called D_2 ansatz are highlighted. The transition from a minimum energy localized amide I state to a fully delocalized state is shown to operate in four phases, one of which is abrupt and the last of which is a fast but smooth change from a very broad yet localized state to a completely delocalized one. Exploration of the dynamical phase space at zero temperature includes the well-known soliton propagation as well as double and triple discrete breathers, and dispersion of initially localized states. The uncertainties related to the question of the thermal stability of the Davydov soliton are illustrated. A solution to the seemingly endless problem of the short radiative lifetime of the amide I excitations is proposed.

1. INTRODUCTION

The Davydov model describes how the energy released in the chemical reaction of hydrolysis of adenosine triphosphate (ATP) can travel from the active site of the enzyme that catalyzed it to other regions of the same protein, while avoiding dispersion and dissipation on the way.[1–10] Following McClare's proposal,[11] in the Davydov model the carrier state is assumed to be a well-known vibrational mode of the amide group H-N-C═O, known as amide I, which consists essentially of the stretching of the C═O bond.[12] Furthermore, the amide I propagation is driven by the dipole-dipole interactions between amide groups, a resonant mechanism which explains the lack of dissipation. Scott, an author who pioneered the studies of the discrete version of the Davydov model[13–20] and who became acquainted with this model during a talk by Davydov, was immediately very impressed because all the parameters in the model, except one, could be estimated independently, this at a time when parameters in physical models of biological phenomena were mostly adjusted to fit experimental data. The parameter that was (and is still) more uncertain is that which describes the interaction of C═O groups with the hydrogen bonds that connect them, which is designated by χ below.

One early objection to McClare's suggestion[11] was the lifetime of vibrational excitations,[4] which in many cases is in the sub-picosecond timescale, too short to be of biological use. The main purpose of the Davydov model was precisely to provide a solution to such short lifetimes. The early work by Davydov and co-workers was concerned with the propagation of amide I vibrations in protein α-helices, represented as a continuum medium. This allowed for exact analytical solutions according to which the amide I travelled along the one-dimensional chains that stabilize α-helices in a self-trapped state, known as the Davydov soliton.[1–10,13,20] It was thought that as a Davydov soliton, the amide I vibrations would have a greater lifetime than when isolated, thus solving the initial objection to McClare's suggestion.

This article revisits the development of the Davydov model, emphasizing what is known and what remains controversial, and ends with a suggestion that overcomes the never ending problem of the short lifetime of vibrational excitations. In Sec. 2 the Hamiltonian first proposed by Davydov[1–4] is described and the early studies are summarized. In Sec. 3 the equations of motion in the mixed quantum-classical regime in which the amide I is treated quantum-mechanically but the lattice is treated classically are derived in an exact manner, showing that the dynamics depends on just two parameters, designated by v and m. In Sec. 4 the physical meaning and validity of the mixed quantum-classical regime are analyzed. In Sec. 5 the transition of the thinly localized stationary

states to broader localized states and ultimately to delocalized states is presented. In Sec. 6 the dynamics that can be obtained with different values of v and m is illustrated and in Sec. 7 the influence of a rising temperature on the latter dynamics is shown. In Sec. 8 the experimental evidence for the Davydov model is shortly re-assessed and in Sec. 9 a role for the decay of amide I excitation is proposed. In Sec. 10 the most important points in this work are summarized and a table of knowns and unknowns regarding the different theoretical regimes is presented in Sec. 11.

2. THE DAVYDOV MODEL

The systems that interest us are the hydrogen bonded chains that stabilize the α-helix and all the other protein secondary structures. These chains are formed by amide groups, in which the C═O group of amide n in the chain makes a hydrogen bond with group H-N of the next amide group in the chain, forming the hydrogen-bonded chain (HBC), as follows:

$$\begin{array}{ccccccc} \cdots & \text{H-N-} & \cdots & \text{H-N-} & \cdots & \text{H-N-} & \cdots \quad \text{(HBC)} \\ & \text{C═O} & & \text{C═O} & & \text{C═O} & \\ & n-1 & & n & & n+1 & \end{array}$$

The Davydov model describes vibrational energy transport along these one-dimensional chains making use of a Hamiltonian very similar to that used for electrons in polarizable crystals. Indeed, the Davydov Hamiltonian $\hat{H}$ has three main terms:

$$\hat{H} = \hat{H}_{\text{ex}} + \hat{H}_{\text{ph}} + \hat{H}_{\text{in}}. \tag{1}$$

where $\hat{H}_{\text{ex}}$ is the exciton Hamiltonian, which describes the storage and transfer of an amide I excitation between adjacent sites, $\hat{H}_{\text{ph}}$ is the phonon Hamiltonian, which describes the vibrations of the amide groups n in the one dimensional chain, and $\hat{H}_{\text{int}}$ is the interaction Hamiltonian, which describes the interaction of the amide I excitation with the motions of the lattice sites.

The exciton Hamiltonian $\hat{H}_{\text{ex}}$ will be taken as

$$\hat{H}_{\text{ex}} = \varepsilon_0 \sum_{n=1}^{N} \hat{a}_n^\dagger \hat{a}_n + V \sum_{n=1}^{N} \left(\hat{a}_n^\dagger \hat{a}_{n-1} + \hat{a}_n^\dagger \hat{a}_{n+1} \right). \tag{2}$$

where only amide I interactions between nearest neighbors are considered; ε_0 is the energy of the amide I at equilibrium distance, i.e., when the displacements $\{u_n\}$ (see below) are zero; V is the dipole-dipole interaction energy between site n and sites $n \pm 1$, in which the distance dependence has been neglected; $\hat{a}_n^\dagger(\hat{a}_n)$ is the creation (annihilation) operator for an amide I excitation at site n and N is the number of sites (the amide groups) in hydrogen bonded chain.

The second term in Eq. (1) is the phonon Hamiltonian $\hat{H}_{\text{ph}}$ given by

$$\hat{H}_{\text{ph}} = \frac{1}{2} \sum_{n=1}^{N} \left[\kappa (\hat{u}_n - \hat{u}_{n-1})^2 + \frac{\hat{p}_n^2}{M} \right]. \tag{3}$$

While hydrogen-bonds are best described by Lennard-Jones potentials, which allow for their breaking and reforming, here they are represented by a harmonic potential, $\hat{u}_n$ being the displacement operator from the equilibrium position of site n. Thus, this model is valid only for small oscillations of the hydrogen bond lengths around their equilibrium values $\hat{p}_n$ is the momentum operator of site n, M is the mass of each site, taken to be the same for all sites, and κ is the spring constant of the hydrogen bond.

Finally, the interaction Hamiltonian $\hat{H}_{\text{int}}$ is

$$\hat{H}_{\text{int}} = \sum_{n=1}^{N} \left[(\chi^+ (\hat{u}_{n+1} - \hat{u}_n) + \chi^- (\hat{u}_n - \hat{u}_{n-1})) \hat{a}_n^\dagger \hat{a}_n \right], \tag{4}$$

where $\chi^+(\chi^-)$ is the variation of the amide I energy ε with distance between site n and the next (previous) site. Again, only small changes with respect to the equilibrium values are considered and the energy dependence on the hydrogen bond length is assumed to be linear. Since we consider periodic boundary conditions, each amide group is linked to two others, both of which will in principle have an influence on the amide I energy. However, since the amide I is essentially a vibration of the C═O group, the hydrogen bond to the amide group that follows has a much greater influence than the hydrogen bond to the group that precedes it (see HBC above). For a more straightforward connection with previous works,[9,21–23] in the dynamical simulations of Secs. 6 and 7.2, we will set $\chi^+ = \chi^- = \chi$. On the other hand, in Sec. 5 the calculation of minimum energy states is made also for $\chi^- = 0$.

As stated above, the parameters in the Davydov model are largely fixed by independent measurements and calculations. The amide I energy ε is measured in optical absorption experiments and has different average values for the two main protein secondary structures[12] but is actually not relevant for the dynamics, as shown in the next section. The dipole-dipole interaction V is calculated with the classical expression well-known from electromagnetism,[24,25] using the dipole moment which was determined to be approximately 0.3 D by Nevskaya and Chirgadze.[26] In the simulations of Secs. 6 and 7, the value of 8 $\text{cm}^{-1} \approx 1.55 \cdot 10^{-22}$ J that has been mostly used for longitudinal interactions along a single chain will be adopted. The elasticity constant of the hydrogen bond has been calculated theoretically to be 19.5 N/m,[27] similar to that estimated experimentally from the vibrational spectra of crystalline formamide, namely, 13 N/m,[28] which is applied in most studies. Also as in many other studies, all the sites have the same mass and the value is the average mass of the amino acids that constitute myosin, as calculated by Scott,[15] i.e., $1.9 \cdot 10^{-25}$ kg. Finally, the parameter which is most difficult to determine is that which describes the variation of the amide I energy ε with the length of the hydrogen bond to which C═O group is attached (if it is not attached, the energy is simply ε_0). Indeed, quantum calculations give rather different values, and sometimes positive and other times negative, according to the level of theory used and according to the basis set chosen.[20,27,29–31] In Secs. 6 and 7 two values will be considered, one of which is 62 pN, the value estimated from experimental data by Careri and Scott[32] and the second one of which is 35 pN, recently used in Ref. 23. All these parameters used in the dynamical simulations are summarized in Table I below.

TABLE I. Parameter values and corresponding physical units.

Variables	α-helix chain	Reference 23
J	$-1.55 \cdot 10^{-22}$ J	$-1.55 \cdot 10^{-22}$ J
κ	13 N/m	13 N/m
M	$1.9 \cdot 10^{-25}$ kg	$1.9 \cdot 10^{-25}$ kg
χ	62 pN	35 pN
1/ Ω (time unit)	0.121 ps	0.121 ps
χ^2 / κ (energy unit)	$2.957 \cdot 10^{-22}$ J	$0.9423 \cdot 10^{-22}$ J
v	−0.524	−1.645
m	2.95	9.25

In Eqs. (1)–(4) the motion of the amide I vibration and of the amide sites are both treated quantum mechanically. To derive equations of motion, in many cases ansätze are made with regard to the wavefunction.[9,10,33] The most popular is arguably the following product ansatz, known in the literature as the D_2 ansatz:

$$|D_2\rangle = \left[\sum_{n=1}^{N}\phi_n(t)\hat{a}_n^{\dagger}|0\rangle_{\mathrm{ex}}\right] \times \left[\exp\left(-\frac{i}{\hbar}\sum_{n=1}^{N}\left(\beta_j(t)\,\hat{p}_n - \pi_j(t)\hat{u}_j\right)\right)|0\rangle_{\mathrm{ph}}\right], \quad (5)$$

where $|\phi_n(t)|^2 = \left\langle \hat{a}_n^{\dagger}\hat{a}_n \right\rangle$ is the probability for the amide I excitation to be in amide group n, $\beta_j(t) = \langle \hat{u}_j \rangle$ and $\pi_j(t) = \left\langle \hat{p}_j \right\rangle$, $\langle \cdots \rangle$ indicating average over the wave function [which in this case is D_2 (5)].

The equations of motion derived by Davydov[1–4,9] for the probability amplitudes $\phi_n(t)$ and for the displacement and momentum averages $\beta_j(t)$ and $\pi_j(t)$, respectively, are exactly the same as those obtained when the motions of the amide groups are treated classically (see the next section). On the other hand, they differ from the equations of motion that are obtained by an exact quantum mechanical derivation which makes use of the time-dependent Schrödinger equation and Ehrenfest equations.[34] However, the difference is only by a phase factor which can be extracted by a gauge transformation of the probability amplitudes ϕn, and which does not affect the values of $|\phi n\,(t)|^2$, $\beta_j\,(t)$ and $\pi_j\,(t)$.

3. THE MIXED QUANTUM-CLASSICAL DAVYDOV MODEL

In the mixed quantum-classical Davydov model the lattice motion is treated classically and thus the displacements and momenta of the sites are real variables, hence-forward designated by u_n and p_n, respectively, where the lack of "hats" above the variables signals their now classical physics nature. One advantage of the mixed quantum-classical regime is that, contrary to the full quantum regime, it is not necessary to invoke ansätze for the wave function as its exact expression is[35,36]

$$|\psi(t)\rangle = \sum_{n=1}^{N}\phi_n(\{u_n\},\{p_n\},t)\hat{a}_n^{\dagger}|0\rangle_{\mathrm{ex}}, \quad (6)$$

where ϕ_n is, as before, the probability amplitude for an amide I excitation at amide group n, whose dependence on the displacements $\{u_n\}$ and momenta $\{p_n\}$ of all the sites need not be specified *a priori*. The normalization condition for the wave function $|\psi(t)\rangle$ implies that $\sum_{n=1}^{N}|\phi_n|^2 = 1$.

That (6) is a general solution of the Hilbert space associated with the mixed quantum-classical Davydov Hamiltonian—obtained from Eqs. (1)–(3) by substituting the operators $\hat{u}_n$ and $\hat{p}_n$ by the corresponding real variables u_n and p_n—can be shown by applying the latter to (6) and verifying that the resulting wave function is still a superposition of the basis states $\hat{a}_n^{\dagger}|0\rangle_{\mathrm{ex}}$, just as (6).

In the mixed quantum-classical regime the displacements and momenta can be considered as time dependent parameters which affect the eigenstates of the quantum particle (the amide I excitation). This regime is also designated as "semiclassical", and is sometimes further associated with the adiabatic approximation, used by Davydov to obtain analytical solutions[1,4,8,9] (see below). However, it should be noted that while in the adiabatic approximation the kinetic energy of lattice sites is considered to be a slowly varying quantity, or is neglected, the wave function in (6) may include the adiabatic case but is not limited to it.

The equations of motion for the probability amplitudes ϕn in the mixed quantum-classical are derived from Schrödinger's equation leading to

$$i\hbar\frac{d\phi_n}{dt} = \varepsilon_0 + H_{\mathrm{ph}} + V(\phi_{n+1} + \phi_{n-1}) + \chi(u_{n+1} - u_{n-1})\phi_n, \quad (7)$$

where H_{ph} is given by the expression obtained after substituting the operators $\hat{u}_n$ and $\hat{p}_n$ in Eq. (3) by the corresponding classical displacements and momenta, as in Eq. (8) below.

On the other hand, the equations for the displacements and momenta are derived from Hamilton's equations applied to the energy functional $\mathcal{E}$ given by

$$\mathcal{E} = \langle\psi|\hat{H}|\psi\rangle = \varepsilon_0 + V\sum_{n=1}^{N}\left[\left(\phi_n^{*}\phi_{n-1} + \phi_n^{*}\phi_{n+1}\right)\right] + \frac{1}{2}\sum_{n=1}^{N}\left[\kappa(u_n - u_{n-1})^2 + \frac{p_n^2}{M}\right] + \chi\sum_{n=1}^{N}\left[(u_{n+1} - u_{n-1})|\phi_n|^2\right]. \quad (8)$$

Indeed, making use of the Hellmann–Feynman theorem (see, e.g., Ref. 37, p. 298):

$$\frac{du_n}{dt} = \frac{\partial\mathcal{E}}{\partial p_n} = \left\langle\psi\left|\frac{\partial\hat{H}_{qc}}{\partial p_n}\right|\psi\right\rangle, \quad (9)$$

$$\frac{dp_n}{dt} = -\frac{\partial \mathcal{E}}{\partial u_n} = -\left\langle \psi \left| \frac{\partial \hat{H}_{qc}}{\partial u_n} \right| \psi \right\rangle, \tag{10}$$

where $\hat{H}_{qc}$ is the mixed quantum-classical Hamiltonian obtained after substituting the operators $\hat{u}_n$ and $\hat{p}_n$ in Eqs. (1)–(4) by the corresponding classical displacements and momenta. From Eq. (10) we get the equation of motion for the displacements u_n

$$M\frac{d^2u_n}{dt^2} = \kappa(u_{n+1} + u_{n-1} - 2u_n) + \chi(|\phi_{n+1}|^2 - |\phi_{n-1}|^2). \tag{11}$$

Equations (7) and (11) constitute the two main equations of motion of the mixed quantum-classical Davydov model. Comparing them with Eqs. (17) and (25) in Ref. 34, which are the equations of motion derived from the D_2 ansatz (5), in an exact quantum-mechanical derivation, it is immediately apparent that the variables $|\phi_n|^2$, u_n, and p_n as predicted by Eqs. (7) and (11), are exactly the same as the supposedly fully quantum variables $|\phi_n|^2$, β_n, and π_n, predicted by Eqs. (17) and (25) in Ref. 34. That is, the two sets of equations are completely equivalent, from the point of view of dynamics.

On the one hand, it is not surprising that the apparently full quantum dynamics predicted by the D_2 ansatz is the same as that predicted by the mixed quantum-classical regime. After all, the only difference between the two regimes is that in the latter the lattice is treated classically and, in the D_2 ansatz, the wave function for the lattice is a coherent state, which is a minimum uncertainty state and thus the quantum state that is closest to the classical state. On the other hand, the D_2 ansatz is a product ansatz, which can neglect correlations between the amide I motions and the site motions, while the wave function $\psi(t)$ (6) makes full allowance for those correlations. In fact, ϕ_n in $\psi(t)$ is itself a correlation, namely, it is the probability amplitude for an amide I excitation to be in site n for a given set of displacements $\{u_n\}$ and momenta $\{p_n\}$.

Equations (7) and (11) are strange in that they couple real site displacements u_n at a given instant to the mere probability amplitude for an amide I excitation to be in site n at that moment. Although this strangeness is necessarily associated with the mixed quantum-classical character of the regime, a similar strangeness appears in the equations of motion derived from the D_2 ansatz. Indeed, in that case it is the averages β_n that are coupled to the same probability amplitudes, constituting yet another sign of the similarity between the two systems of equations.

Proceeding now as in Ref. 38, let us transform the equations of motion (7) and (11) into non-dimensional equations by rescaling the time t and the displacement variables u_n to dimensionless variables as follows:

$$\tau = \Omega t, \quad \Omega = \sqrt{\frac{\kappa}{M}}, \quad q_n = \frac{\kappa}{\chi}u_n, \tag{12}$$

where $1/\Omega$ is the unit of time, χ/κ the unit of length and χ^2/κ the unit of energy. Making the gauge transformation $\varphi_n = e^{-\frac{i}{\hbar}(\varepsilon + H_{ph})t}\phi_n$, and defining two new variables, v and m as

$$v = \frac{V}{\chi^2/\kappa}, \quad m = \frac{\hbar\Omega}{\chi^2/\kappa}. \tag{13}$$

Equations (7) and (11) become

$$im\frac{d\varphi_n}{d\tau} = v(\varphi_{n+1} + \varphi_{n-1}) + (q_{n+1} - q_{n-1})\varphi_n, \tag{14}$$

$$\frac{d^2q_n}{d\tau^2} = (q_{n+1} + q_{n-1} - 2q_n) + (|\varphi_{n+1}|^2 - |\varphi_{n-1}|^2). \tag{15}$$

Although the initial Hamiltonian (1)–(4) included five different physical parameters, namely, ε_0, J, M, κ, and χ, Eqs. (14) and (15) show that, in the absence of thermal baths, the dynamics of the mixed quantum-classical system, as well as the dynamics of the full quantum system as predicted by the D_2 ansatz, can be classified in terms of two parameters only, namely, v and m. As in the case of Davydov's investigations,[1–7,13] the derivation of Eqs. (14) and (15) did not include a perturbation approximation and thus they are valid for all values of those two parameters. As pointed out in the introduction, one strong point of the Davydov model is that, except for the nonlinearity parameter χ, the values of the parameters can be determined independently. In Sec. 6, we explore two different dynamical possibilities corresponding to the two sets of parameters displayed in Table I. The set denominated α-helix includes the most commonly used values in numerical simulations[13,20,21] and the second set has been used in recent publications.[23] When combined, they correspond to four extremes of the parameter space and thus provide a good overview of the dynamical possibilities.

4. FURTHER THOUGHTS ON THE VALIDITY OF THE MIXED QUANTUM-CLASSICAL DAVYDOV MODEL

We have seen that although dynamics with the D_2 ansatz starts in the full quantum regime it ends in the mixed quantum-classical one. Therefore, it is important to establish the range of validity of the mixed quantum-classical Davydov model. In this section this is done by comparing the predictions of the latter model to those of the full quantum Davydov model which constitutes the absolute reference.

It should first be said that, although not calling it by this name, the early papers by Davydov and co-workers[1–5] do deal with the mixed quantum-classical regime, by applying not only of a wavefunction exactly like (6) but also deducing the equations of motion for the sites from an energy functional equivalent to (8). The studies employing the D_2 ansatz were published later. [8,9,39,40] Thus, the equivalence between the equations obtained with the D_2 ansatz and those obtained earlier within the mixed quantum-classical regime is already apparent in the work of Davydov and co-workers.

In spite of the strangeness of the mixed quantum-classical equations of motion mentioned in the previous section, there are more reasons, besides its formal equivalence to the predictions of the D_2 ansatz, to justify its application to the hydrogen bonded chains of amide groups. First, it is clear that the amide I excitations

must be treated quantum mechanically. Indeed, the average lattice compression correlated with the position of the excitation obtained with the fully classical Davydov system, in which the amide I is also treated classically,[41] is much smaller in absolute terms than the corresponding averages obtained in the mixed quantum-classical system.[42] Also very different are the absorption spectra of amide I in α-helix chains obtained for those two regimes, with the full classical spectrum being much thinner than the mixed quantum-classical one, and with the latter proving a much better fit to the protein α-helix spectra obtained experimentally.[35] Secondly, it is less clear that the lattice has to be treated quantum mechanically. A priori the mass of the amino acid sites in an α-helix, and the fact that biological systems function at 310 K, for which the Bose–Einstein distribution of the phonons is virtually similar to the Boltzmann distribution for the frequencies involved, are two reasons for the lattice to behave classically.

Another argument in support of the validity of the mixed quantum-classical regime is the fact that, above 10 K, the average lattice distortion calculated by full quantum Monte Carlo methods[22] is virtually indistinguishable from the average distortion calculated by an exact mixed quantum-classical approach, for the same values of all parameters.[42] Furthermore, dynamical simulations of the fully quantum Davydov monomer at finite temperature also compare well with the corresponding simulations of the mixed quantum-classical monomer.[43]

Taken together, the above arguments suggest that the mixed quantum-classical Davydov model is at least a good starting point to study the propagation of amide I vibrations in the chains of hydrogen bonded peptides. Two of its advantages is that the derivation of the equations of motion does not require neither an ansatz for the wave function nor a perturbative approach so that its predictions are valid for any value of v, i.e., from the small soliton to the large soliton, all the way to completely delocalized solutions, as it will be clear in the next section.

5. THE STATIONARY STATES OF EQS. (14) AND (15)

Inserting in Eq. (14) a stationary solution of the form

$$\varphi_{nj}^{\mathrm{st}} = A_{nj}\exp(-tE_j\tau), \tag{16}$$

in which A_{nj} is not dependent on time, we get the time-independent Schrödinger equation (for the case, in which $\chi^- = 0$):

$$mE_jA_{nj} = v(A_{n+1j} + A_{n-1j}) + (q_n - q_{n-1})A_{nj}, \tag{17}$$

from which we can find the band E_j of amide I states associated with a given set of displacements $\{q_n\}$. Below we shall see one application of this equation.

In order to get analytical expressions, Davydov further considered the case in which the momenta are zero or vary slowly,[1–10] i.e., when $d^2q_n/d\,\tau^2 \approx 0$ in Eq. (15) which leads to

$$q_n - q_{n-1} \approx -|\varphi_n|^2. \tag{18}$$

Substituting the latter result in (14) we obtain the so-called discrete nonlinear Schrödinger equation

$$im\frac{d\varphi_n}{d\tau} = v(\varphi_{n+1} + \varphi_{n-1}) - |\varphi_n|^2\varphi_n, \tag{19}$$

whose stationary solution is Ref. 20

$$|\varphi_n|^2 = \frac{1}{8|v|}\,\mathrm{sech}^2\left(\frac{n-n_0}{4|v|}\right). \tag{20}$$

In the absence of interaction between the amide I excitation and the vibrations of the amide groups, i.e., when $\chi = 0$, the amide I states are just Bloch states, with $|\varphi_n|^2 = 1/N$, and the amide group motions are uncorrelated with it and at $T = 0$ K their displacements q_n are equal to zero. Also the energy of the minimum energy state is just $-2v$. On the other hand, when $\chi \neq 0$, Eq. (20) tells us that the stationary state for the amide I is pulse-like and v is a measure of its width. Also, correlated with the pulse-like amide I excitation there is a local compression of the chain, given by (18), and which travels with it. This is a mathematical expression of the Davydov soliton.

We can also determine the stationary states of the mixed quantum-classical Davydov model directly from the minimization of the dimensionless functional $\mathcal{E}'$ given by

$$\mathcal{E}' = (\mathcal{E} - \varepsilon_0)/(\chi^2/\kappa) = v\sum_{n=1}^{N}\left[\left(\varphi_n^*\varphi_{n-1} + \varphi_n^*\varphi_{n+1}\right)\right] + \frac{1}{2}\sum_{n=1}^{N}(q_n - q_{n-1})^2 + \sum_{n=1}^{N}\left[(q_{n+1} - q_n)|\varphi_n|^2\right], \tag{21}$$

where the kinetic energy of the amide groups has been dropped since a minimization with respect the momenta is trivially achieved by setting all of them equal to zero. Therefore, the numerical minimization of $\mathcal{E}'$ can just be done with respect to the non-dimensional displacements q_n and to the probability amplitudes φ_n which must obey the non-linear constraint:

$$\sum_{n=1}^{N}|\varphi_n|^2 = 1. \tag{22}$$

Figure 1 compares the numerically obtained minimum energy states (black curve) with the corresponding analytical solutions given by (20) (red curve).

The analytical expression is valid for amide I states for which the width of the probability distribution covers a sufficiently large number of sites. Figure 1 shows that at very low values of v, when the distribution is very localized, the analytical expression (20) slightly overestimates the width of probability distribution, but as v increases, the analytical expression becomes a good approximation of the exact numerical result. For $v = 0$ (not shown) the wave function is completely localized at one site and, as expected, as v increases, the wave function gets increasingly broader. However, in spite of this monotonic increase of broadness, the rate at which it occurs also varies with v. Indeed, noticing that the y scale in Fig. 1 is successively smaller going down from row to row, it becomes

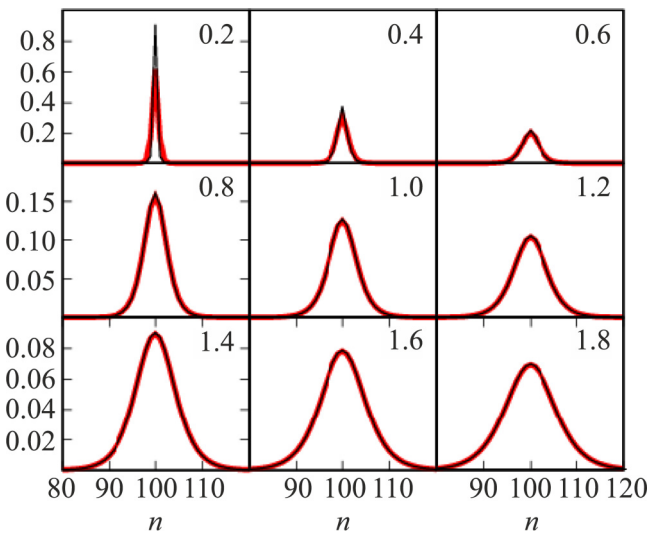

FIG. 1. Minimum energy states calculated from [(20), red curve] and from numerical minimization of [(21), black curve]. The values of v are specified at the top right of each plot. For the numerical states, $N = 200$.

apparent that the increase in broadness as v increases is first faster and then proceeds more slowly. Figure 2 shows this more clearly.

The stationary solution (20) (and also the moving solutions) first determined by Davydov[1–6] lead to localized states for the amide I, however broad, as long as $\chi \neq 0$. Therefore, it was a surprise when the numerical simulations performed by Scott and co-workers showed that a soliton only formed above a critical value of χ[13] It was later shown that soliton formation depends on the initial condition[9,44] (which also defines the energy level since the Davydov Hamiltonian (1)–(4) is conservative). That is, the threshold value obtained by Scott and co-workers[13] applies when the initial condition is a single site excited initially, but for a different initial condition, its value may well be different, as shown by the dynamical simulations in Secs. 6 and 7.2. In Fig. 2 the infinite space of initial conditions we can choose from is avoided by considering always the minimum energy states, for each value of v. From the insets in Fig. 2 we see that the threshold value of v, when $\chi^- = \chi^+ = \chi$ is approximately four times the value it has when $\chi^- = 0$. Indeed, setting $\chi^- = \chi^+ = \chi$ is roughly equivalent to having $\chi^- = 0$ and $\chi^+ = 2\chi$.

The existence (or not) of an abrupt transition from the localized state to the delocalized state has been much discussed in the literature.[9,36,45–50] In Ref. 49 the variation of the binding energy of the soliton versus v and N was used to monitor the transition, while in Ref. 36 it was suggested that the reason for the abruptness of the transition from broad localized to completely delocalized is that this transition happens when the size of the chain becomes too short to hold a too broad amide I state. And so, as the number of sites N decreases, this transition takes place at successively lower values v and also seems increasingly abrupt. On the other hand, as N increases, the transition takes place at higher values of v and becomes smoother, and when $N \to \infty$ it is abolished, as happens in the continuum case.

Figure 2 confirms the previous reasonings, but also shows that the situation is more complex than previously thought. Both plots in Fig. 2 show that the transition from localized states to a delocalized one has three inflexion points. Indeed, the decrease in localization as v increases from zero is first slow, then becomes faster until it slows down again at $v \approx 2$ for $\chi^- = \chi^+$ (a) and at $v \approx 0.5$ for $\chi^- = 0$. The third inflexion point is when the peak of the probability distribution suddenly becomes very close to $1/N$, the value it has in a completely delocalized state. The evolution from this localized, but very broad state, to the completely delocalized is then fast, but smooth. In short, there are four phases in the transition from a

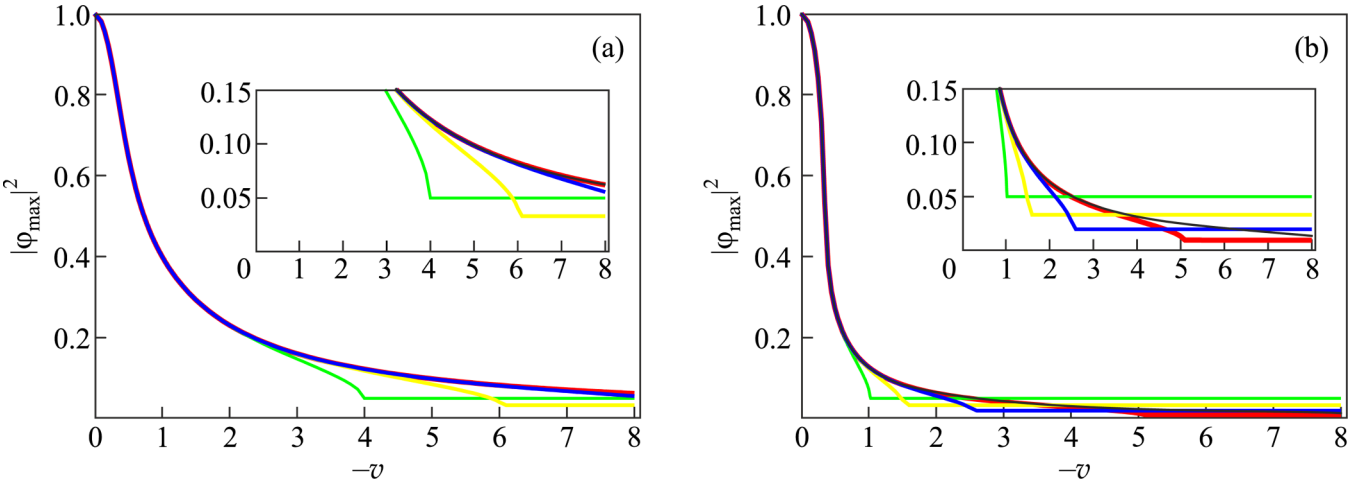

FIG. 2. Maximum value of $|\varphi_n|^2$ as function of v, for N: 20 (green curve), 30 (yellow curve), 50 (blue curve), 100 (red curve), and 200 (black curve); for $\chi^- = \chi^+$ (a) and for $\chi^- = 0$ (b).

thinly localized amide I state to a completely delocalized one, and two are smooth, one is fast and another is abrupt. The abrupt one is the change from a broad localized state to an almost completely delocalized state. In the infinite chain considered in the continuum models[1–10] the states can be as large as necessary and thus the abrupt transition is suppressed. The surprise is nevertheless that the abrupt transition is not to a completely delocalized state but instead to a localized, but very broad state, which then evolves very fast but smoothly to the delocalized state.

5.1. The soliton band

The minimum energy state discussed until now corresponds to finding the set of site displacements $\{q_n\}$ and amide I probability amplitudes $\{\varphi_n\}$ which minimize the functional $\mathcal{E}'$ (21). In Fig. 1 only the probability distribution of the amide I state was shown, but associated with it there is a corresponding set of site displacements, as shown in Fig. 3.

All the results presented in this work were obtained with periodic boundary conditions. The peaks of localized stationary states are all positioned at the middle of the chain, but they would represent exactly the same state if positioned at another site, provided amide I probabilities $|\varphi_n|^2$, the site displacements q_n (and consequently also the displacement differences) were all shifted by exactly the same amount. That is, from the point of view of translation along the chain, there is a degeneracy of order N for each state. On the other hand, for each set of site displacements q_n, we find N eigenstates for the amide I vibration, of which the minimum energy state is just the eigenstate with the lowest energy. In Fig. 4 the $N = 20$ amide I states associated with the lattice distortion of the minimum energy state for $v = 0.524$ are displayed, something that shall be designated here as the soliton band.

For $v \neq 0$ and with values for which the minimum energy state is localized, Fig. 4 provides a good illustration of the general features of the soliton bands we can encounter for finite values of N. Apart from the minimum energy, soliton state, on the top left panel, we find $N-1$ states with higher energy, some of which are also soliton-like, as level 2 and level 20 in Fig. 4. However, while the minimum energy amide I state is a bright soliton, with a peak in the middle, these higher energy localized states are in the form of dark solitons, with a trough in the middle. In fact, it is found that when the lowest amide I eigenstate is a bright soliton, the highest is always a dark soliton. Finally, most of the states with intermediate energies are extended, exciton-like states, in which the amide I probability distribution has an oscillatory pattern along the chain.

The binding energy of the Davydov soliton is usually calculated as the energy difference between completely delocalized, exciton (Bloch) states and the soliton energy.[1–7,10,20] Implicit in this calculation is the assumption that soliton destabilization is via a transition to such an exciton state. Direct transitions between the soliton state and higher energy states in the soliton band are not possible because the states in the band are orthogonal to one another. However, absorption of electromagnetic radiation may cause such transitions, if the energy difference between the states is equal to hν, where ν is the frequency of the applied electromagnetic

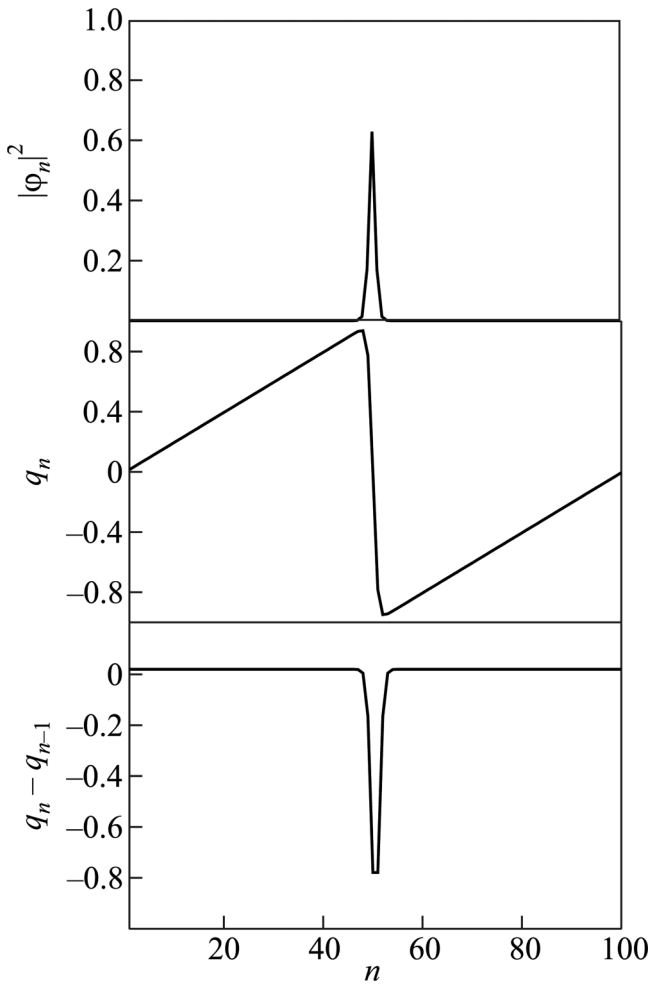

FIG. 3. Minimum energy state for $v = 0.524$. The top plot shows the probability of an amide I excitation in site n, $|\varphi_n|^2$, the middle plot shows the displacements of each site n, q_n, and the bottom plot shows the displacement differences (the local lattice compression) at site n, $q_n - q_{n-1}$.

waves. Such transitions have at least a very favorable Franck–Condon factor because the lattice conformation is the same for the initial and final amide I states. Thus, the transitions to states in this band may be important when dealing with the influence of electromagnetic fields on solitons.[51–54]

6. DYNAMICS AT LOW TEMPERATURE

Stationary states, when inserted in the equations of motion (14) and (15), in the absence of perturbations (like thermal baths) remain always at the same site. One way to test the eigenstates discussed in the previous section is precisely to insert them in the Eqs. (14) and (15) and verify that they do not move and do not change. On the other hand, in cells, the amide I is supposed to arise because of the chemical reaction of hydrolysis of ATP, or

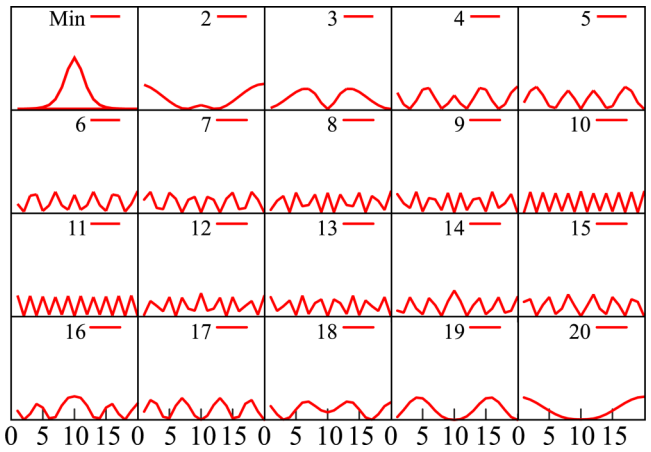

FIG. 4. Soliton band for $v = 0.524$ in a chain with $N = 20$ sites. In each panel is plotted the probability distribution $|\varphi_n|^2$ for each of the 20 amide I eigenstate associated with the soliton lattice distortion. The amide I energy levels increase from left to right and from top to bottom, starting with the minimum energy (soliton) state. The title of each plot is the energy level.

because of the binding of a ligand to a protein,[55] so it may not be in an eigenstate to start with. In this section we consider four different initial conditions: one in which the amide I excitation is initially in one site only, as in Refs. 13 and 21, a second one in which the amide I distribution is a truncated Gaussian pulse[23] and two minimum energy solutions obtained numerically (see Sec. 5), for $v = -0.524$ which is one of the most used values in the literature,[13,20,21] and for $v = -1.645$,[23] and explore the dynamics for the amide I and the amide groups in the chain, as predicted solely by Eqs. (14) and (15), i.e., in the absence of thermal baths.

In Fig. 5 the initial condition in the panel on the bottom right is the minimum energy state obtained for $v = -0.524$, the value that is also used in the dynamical Eqs. (14) and (15) in all plots. The perfect conservation (up to numerical accuracy) of the probability distribution $|\varphi_n|^2$ and of the associated lattice contraction (positive in the plot for a more clear view) demonstrates two points: first, the accuracy of the numerical determination of the minimum energy state, and secondly, the accuracy of the integration of the equations of motion which conserve the norm and the total energy at least up to 1 part in 10^{13}, which is also the accuracy for the conservation of each term $\hat{H}_{\rm ex}$ (2), $\hat{H}_{\rm ph}$ (3) and $\hat{H}_{\rm int}$ (4) in the Hamiltonian (1), as expected for true stationary states. The total kinetic energy of the phonons is zero, which, when defined with the same accuracy 1 part in 10^{13} leads to oscillations in the momenta of the order of 10^{-7}, as shown in Fig. 5. Notice that the scales may differ from one panel to another and that if the momenta p_n of the bottom right of Fig. 5 were plotted using the same scale as the other plots they would be portrayed as perfect flat lines, corresponding to $p_n = 0$, as expected for an exact minimum energy state. In this and all of the other plots in this work the total time is 524.288 time units, which, with the parameters in Table I corresponds to 63.44 ps.

The other three initial conditions are not stationary states for $v = -0.524$ and thus they change with time. But comparing the probability distributions of the latter plots with that of the exact minimum energy state we see that the changes suffered by the non-stationary states have the general trend of tending to a distribution closer to the minimum energy state. That is, when the starting probability distribution $|\varphi_n|^2$ has a peak value greater than the 0.7 value of the minimum energy state, like that of the top left plot, the evolution leads to distributions with lower peak values, and vice-versa, when the initial condition has a peak value smaller than value of the minimum energy state, like those of the top and bottom right plots, the evolution leads to distributions with larger peak values.

Another common trend of the zero temperature dynamics is that the tendency to acquire a form closer to the corresponding minimum energy state is achieved through breather-like motion of both the probability distribution and of the lattice contraction. Similar dynamical states were found in velocity driven minimum energy states and were denominated double (discrete) breathers[36] (double because not only the lattice sites[56,57] but also the amide I state breathes). The plots also show that the non-stationary states suffer a slight dispersion, with emission of phonons which cause both chain compressions and expansions, represented, respectively, by positive and negative lattice displacements in the figures, which move with the sound velocity and are position correlated with the peaks and troughs in the plots p_n.

While the minimum energy states are only dependent on v, the dynamics is dependent also on m [see Eqs. (12) and (14)]. In Fig. 6 the initial conditions and the value of v are the same as in Fig. 5, but m is 9.25. Equations (14) and (15) show that the parameter m can be interpreted as a scaling of time, which affects the dynamics of φ_n more strongly than the dynamics of q_n so it cannot be represented by a simple re-scaling of the time for the whole system. Nevertheless, the general slowing down effect is quite visible in Fig. 6. Indeed, the breathing motion of the amide I probability distributions are now seen much more clearly, but they are coupled to faster breathing motions of the lattice sites. The dynamics of the amide I state at the bottom right plot, which starts with an initial condition for $v = -1.645$ that is a better match of the value of $m = 9.25$ (see Table I) is now a triple breather, with the momenta p_n also oscillating with a frequency approximately two times larger than that of the probability $|\varphi_n|^2$ and the lattice displacements. On the other hand, the dynamics of the exact minimum energy state remains unchanged, as expected.

In Figs. 5 and 6, all localized states (let us call them solitons) remain localized throughout the allotted time interval (which using the parameters in Table I corresponds to 63.44 ps). But their dynamical stability is expected to decrease as v increases in absolute terms and thus in Fig. 7 in which the initial conditions are the same as before, v is now –1.645.

For this larger v (in absolute terms), the state in which the amide excitation is localized at a single site is not dynamically stable and disperses comparatively very fast (top left panel). On the other hand, the truncated Gaussian state is not only stable but also moving (top right panel). It should be noted that this state is constructed to have an intrinsic initial momentum[23] but this had not been apparent in Figs. 5 and 6. For these parameters the truncated

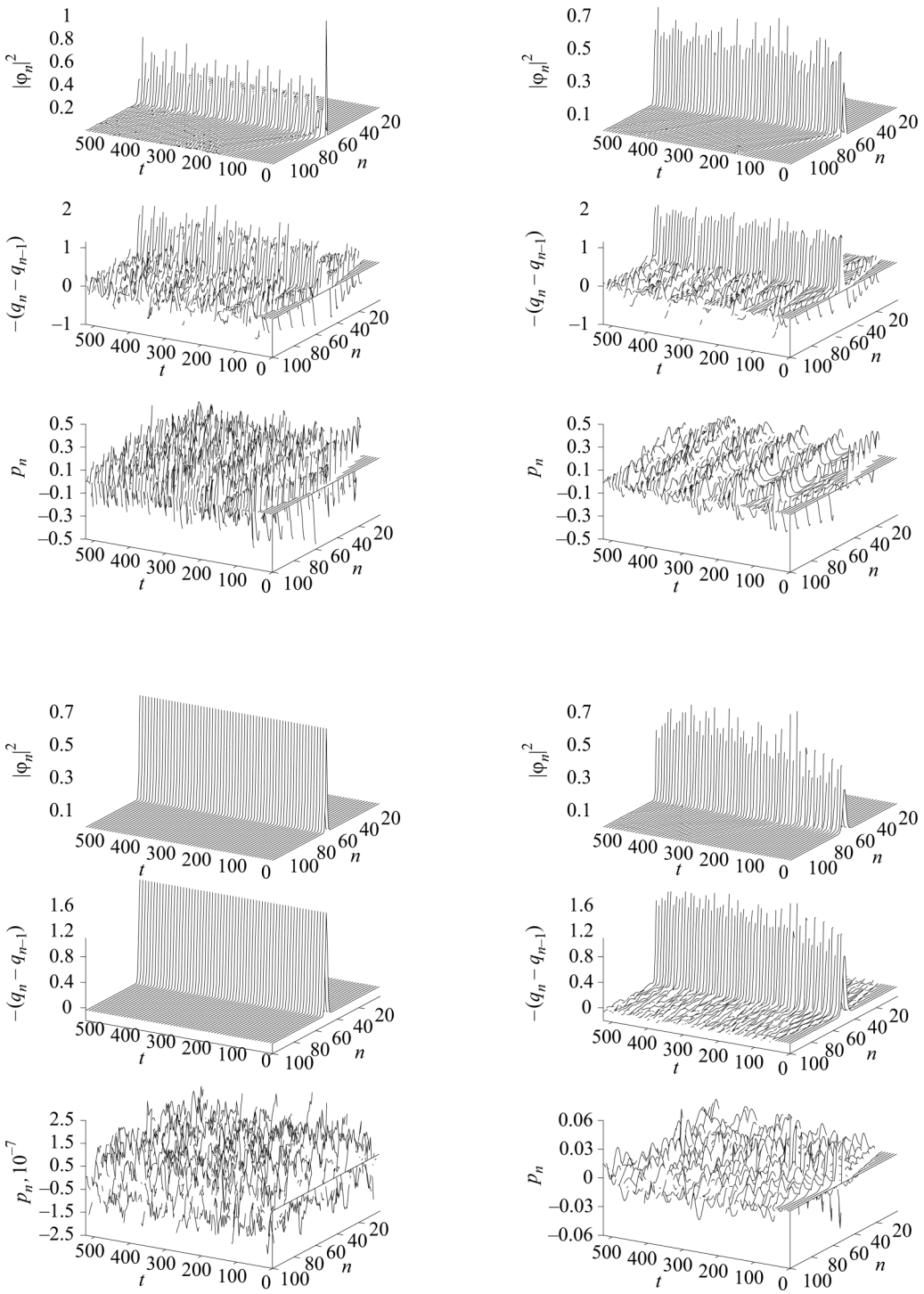

FIG. 5. Zero temperature dynamical evolution with $v = -0.524$ and $m = 2.95$. Initial conditions are: one site excited at $n = 50$ (top left), truncated Gaussian (top right), minimum energy state for $v = -0.524$ (bottom left) and for $v = -1.645$ (bottom right). Equations (14) and (15) have been used. In each panel the top plot displays the probability amplitude for the amide I excitation to be in lattice site n, $|\varphi_n|^2$, the middle plot displays the local contraction of the lattice $-(q_n - q_{n-1})$, and the lower plot displays the momenta p_n of each lattice site, as function of time.

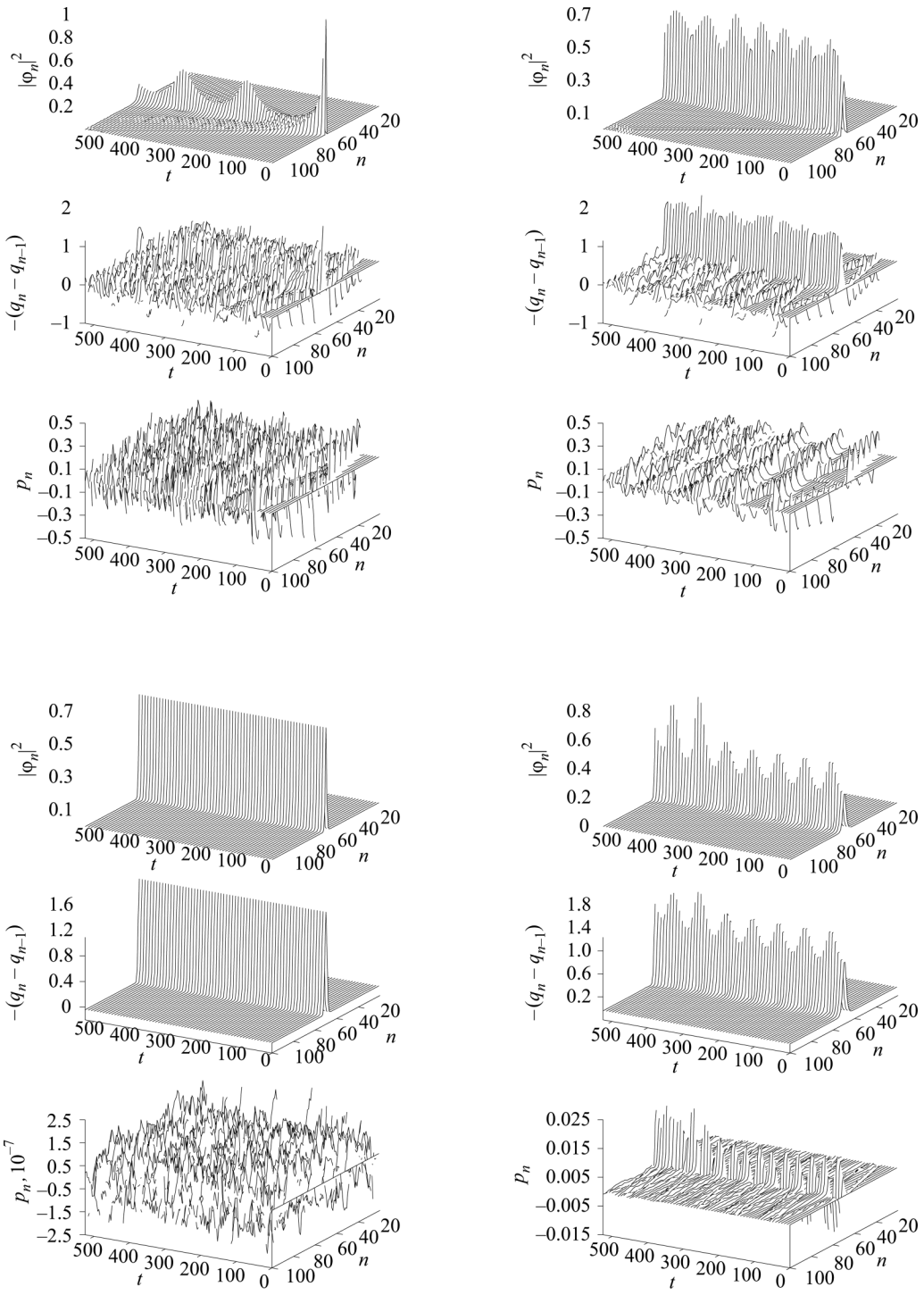

FIG. 6. Zero temperature dynamical evolution with $v = -0.524$ and $m = 9.25$. Initial conditions are: one site excited at $n = 50$ (top left), truncated Gaussian (top right), minimum energy state for $v = -0.524$ (bottom left) and for $v = -1.645$ (bottom right). Equations (14) and (15) have been used. In each panel the top plot displays the probability amplitude for the amide I excitation to be in lattice site n, $|\varphi_n|^2$, the middle plot displays the local contraction of the lattice $-(q_n - q_{n-1})$, and the lower plot displays the momenta p_n of each lattice site, as function of time.

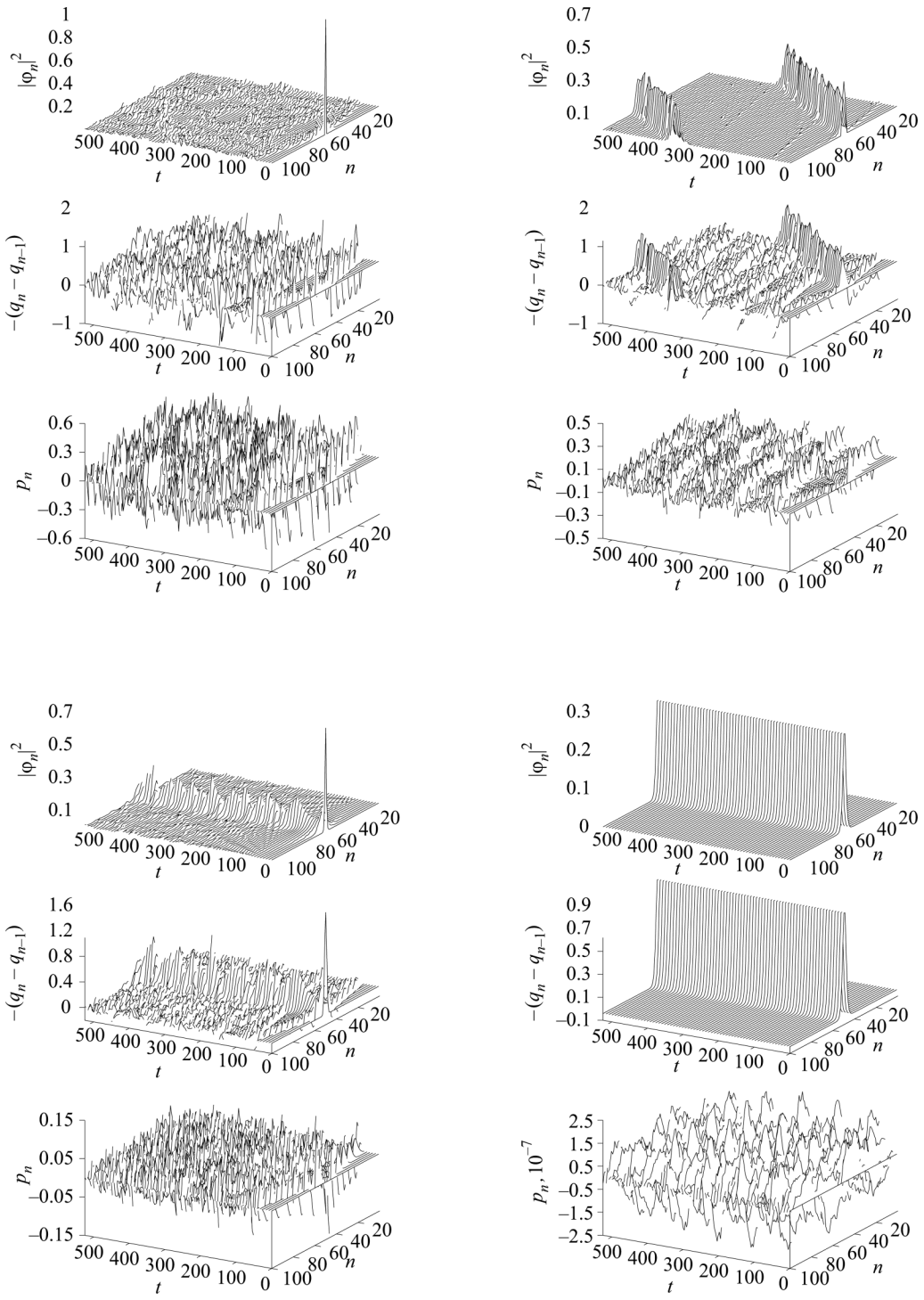

FIG. 7. Zero temperature dynamical evolution with $v = -1.645$ and $m = 2.946$. Initial conditions are: one site excited at $n = 50$ (top left), truncated Gaussian (top right), minimum energy state for $v = -0.524$ (bottom left) and for $v = -1.645$ (bottom right). Equations (14) and (15) have been used. In each panel the top plot displays the probability amplitude for the amide I excitation to be in lattice site n, $|\varphi_n|^2$ the middle plot displays the local contraction of the lattice $-(q_n - q_{n-1})$, and the lower plot displays the momenta p_n of each lattice site, as function of time.

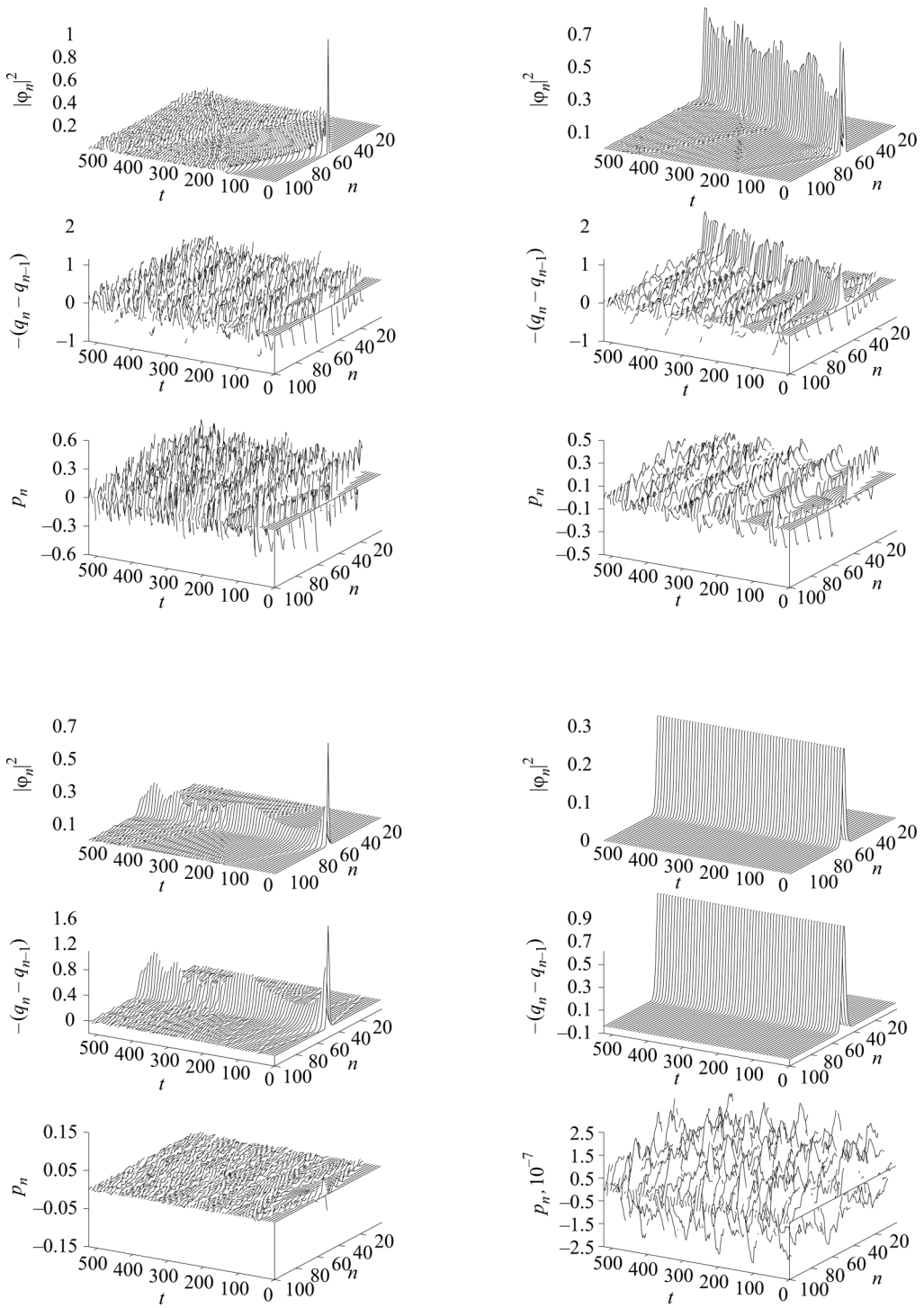

FIG. 8. Zero temperature dynamical evolution with $v = -1.645$ and $m = 9.25$ (see text). Initial conditions are: one site excited at $n = 50$ (top left), truncated Gaussian (see text) (top right), minimum energy state for $v = -0.524$ (bottom left) and for $v = -1.645$ (bottom right). Equations (14) and (15) have been used. In each panel the top plot displays the probability amplitude for the amide I excitation to be in lattice site n, $|\varphi_n|^2$, the middle plot displays the local contraction of the lattice $-(q_n - q_{n-1})$, and the lower plot displays the momenta p_n of each lattice site, as function of time.

Gaussian excitation moves, but there is no correlation of the values p_n with this movement. Indeed, pn correlates instead with the sound waves generated in the lattice which, in turn, correlate with amide I radiation from the main peak. On the other hand, the bottom left plot of Fig. 7 shows the minimum energy state for $v = -0.524$ evolving towards the shape corresponding to the $v = -1.645$ used in the equations of motion. And finally, the minimum energy state for $v = -1.645$ remains perfectly stable because it is an exact stationary state.

For the sake of completion, we now examine the evolution of the same states as before but when $v = -1.645$ and m has the corresponding value of 9.25 (see Table I).

The top right figure shows that the amide I excitation which is initially at a single site does not disperse, as in Fig. 7, but evolves into a pulse with peak size close to 0.3 as the minimum energy state in the bottom right, and, in spite of the radiation this lower peak pulse manages to survive one and a half turn over the ring lattice. However, the noise generated in the lattice motions is dominated by sound waves which correlate with the momenta p_n, so the localized amide I state eventually disperses as expected from Fig. 7. The truncated Gaussian pulse moves and this motion is correlated with a lattice compression, but also quite clear are sound waves in the lattice correlated with the changes in the momenta p_n. Finally, the minimum energy state for $v = -0.524$ in the bottom left panel again evolves to a state closer to the exact stationary state displayed in the bottom right plot, while remaining pinned to the centre site where it was first created.

These results are in full agreement with the conclusions of Brizhik and Davydov who showed that the existence of a threshold for soliton formation and the value of that threshold are dependent on the form of the initial excitation.[44] Here we showed also the dependence of the threshold on the two dynamical parameters v and m whose variation leads to the many types of dynamical evolutions encountered in the dynamics of nonlinear systems.

All the results so far were obtained in the absence of thermal baths, but to be useful in biological systems, the localized amide I states must be robust also at finite temperature. Thus, we now turn to the problem of finite temperature effects, a subject that remains still as controversial as when it was first raised by Lomdahl and Kerr.[21]

7. FINITE TEMPERATURE SIMULATIONS

We have already mentioned that in the continuum approximation, as v increases, the Davydov soliton becomes broader, resembling the exciton state.[1–7] Also, in his studies of the thermal stability of the amide I soliton[9,10,58–60] Davydov concluded that, as temperature increases, the soliton becomes broader, but remains stable. These results naturally lead to the idea that the destabilization of the Davydov soliton is related to a transition to completely delocalized, exciton (Bloch) states. Perhaps because of this, the binding energy of the Davydov soliton, i.e., the energy that must be absorbed by the soliton in order to destabilize it, is usually defined as the energy difference between the lowest energy exciton state, $-2v$ for $N > 2$, and the soliton energy.[1–10,20] However, each set of displacements $\{q_n\}$ is associated with a band of amide I eigenstates and the exciton band is just the band associated with zero displacements. In Sec. 5.1 we have seen the band associated with the lattice distortion of the soliton state. As mentioned previously, a direct transition from the soliton to another state in the same band is not possible because those states are orthogonal to one another. However, if the lattice displacements change because of thermal agitation, the amide I band at time t will be different from the band at time $t' > t$ and transitions between states belonging to the two different bands are allowed. Davydov pointed out that it is not possible to generate a soliton directly by light absorption because the superposition of the initial lattice conformation and that of a soliton state is not favorable[4,6] and a similar argument is valid for the transition from the soliton state to an exciton. But when we consider the changes in the site positions due to thermal agitation the possibility arises of many other transitions from the soliton to a slightly disordered state, and from that to other increasingly disordered ones,[61] whose corresponding energy differences may well be lower than the so-called binding energy of the soliton and whose Franck–Condon factors may also be more favorable if the lattice conformations in the two instants are similar. In fact, in a disordered lattice, there is no exciton band but because of Anderson localization there are many localized states,[36] which provide channels for the thermal destabilization of the soliton state.

In this section we distinguish two regimes: the thermal equilibrium regime and the non-equilibrium regime. While biological processes occur in a non-equilibrium state (equilibrium in biology is only achieved when a cell dies), thermal equilibrium is very useful because it provides an exact reference for the non-equilibrium regime.

7.1. Thermal equilibrium

Let us first consider the case in which both the amide I and the lattice motions are treated classically. The thermal average of a general classical quantity $C_{\rm cl}$ ($\{\varphi_n\}$, $\{q_n\}$) that is a function of the classical complex amplitudes $\{\varphi_n\}$ and of the classical site displacements $\{q_n\}$ can be calculated as follows:

$$\ll C_{\rm d} \gg = \frac{\int_{2N\,\text{unit}-\text{sphere}} \{d\varphi_n^r\}\{d\varphi_n^i\} \int \{dq_n\} \exp(-\beta \mathcal{E}') C_{\rm cl}(\{\varphi_n\},\{q_n\})}{\int_{2N\,\text{unit}-\text{sphere}} \{d\varphi_n^r\}\{d\varphi_n^i\} \int \{dq_n\} \exp(-\beta \mathcal{E}')}, \tag{23}$$

where << … >> denotes thermal average and in dimensionless units $\beta = 1/T'$ (see below). φ_n^r and φ_n^i are, respectively, the real and imaginary parts of the classical amplitudes φ_n and the integration over the 2 N unit-sphere ensures that they remain normalized. Also the integration over the classical momenta $\{p_n\}$ does not appear because the corresponding integral in the numerator cancels with that in the partition function of the denominator.

On the other hand, in the mixed quantum classical regime, in which the lattice is treated classically but the amide I state is treated quantum mechanically, the thermal average of a general quantity $\hat{C}_{\rm qu-cl}(\{\hat{a}_n\}, \{\hat{a}_n^\dagger\}, \{q_n\})$ which is now an operator because it depends on the operators $\hat{a}_n$ and $\hat{a}_n^\dagger$ for the amide I, can be calculated as follows:

$$\ll \hat{C}_{\mathrm{qu-cl}} \gg = \frac{\int^{\{dq_n\}} \exp\left(-\beta H_{\mathrm{ph}}\right) \sum_{j=1}^{N} \exp\left(-\beta E_j\right) \left\langle \psi_j \middle| \hat{C}_{\mathrm{qu-cl}}\left(\{\hat{a}_n\}, \left\{\hat{a}_n^{\dagger}\right\}, \{q_n\}\right) \middle| \psi_j \right\rangle}{\int^{\{dq_n\}} \exp\left(-\beta H_{\mathrm{ph}}\right) \sum_{j=1}^{N} \exp\left(-\beta E_j\right)}, \tag{24}$$

where $\left|\psi_j\right\rangle = \sum_{n=1}^{N} A_{nj} \hat{a}_n^{\dagger} |0>_{\mathrm{ex}}$ is the eigenstate with energy E_j for a given set $\{q_n\}$.

Let us emphasize the difference between the thermal average in the full classical regime, given by (23), and in the mixed quantum-classical regime, (24). While in the mixed quantum-classical average, only the eigenstates of the amide I for a given set of classical displacements $\{q_n\}$ contribute to the thermal average, in the full classical average (23) the integration over the real and imaginary parts of the classical amplitudes φ_n means that all superpositions of eigenvectors contribute to thermal average, as well.

Finally, in the full quantum regime, the displacements and momenta are also operators and an expression for the thermal average of a full quantum quantity $\hat{C}_{\mathrm{qu}}(\{\hat{a}_n\}, \{\hat{a}_n^{\dagger}\}, \{\hat{q}_n\}, \{\hat{p}_n\})$ has been derived in Ref. 35, using Feynman's path integral formulation of Quantum Mechanics. It is rather involved and of no use for this work, but the interested reader can always consult the Ref. 35

These three thermal equilibrium regimes can and have been studied in an exact manner, in the case of the Davydov model.[22,41,42] The important point is that thermal averages, such as can be calculated from (23) and (24) provide a crucial reference for what to expect at finite temperature dynamics. Indeed, non-equilibrium equations such as (25) and (26) below, when run for a sufficiently long time, should drive the system to equilibrium. Thus, for instance, in the full classical regime, the time average of a variable $C_{\mathrm{cl}}(\{\varphi_n\}, \{q_n\})$ should tend to the equilibrium value obtained from (23). In Ref. 41 such a time average of the lattice displacement correlated with the peak in probability distribution of amide I was calculated using (23) and Eqs. (25) and (26) below. The two results were virtually equal which lead to the (wrong) conclusion that the Langevin Eqs. (25) and (26) provided a good description of the mixed quantum classical Davydov system at finite temperature. Since (23) is the thermal average in the full classical regime, what was in fact shown was quite the contrary: even if they are sometimes used to study the thermal dynamics of mixed quantum-classical systems, Langevin equations such as (25) and (26) below lead to a fully classical representation the amide I thermal dynamics.[35] Furthermore, the error involved in the use of Langevin equations can be evaluated by comparing the correct mixed quantum-classical average of the lattice displacement correlated with the position of the amide I excitation using (24)[42] with that obtained with (23).[41] Calculations of the average degree of amide I localization for a dimer show that the Langevin average and consequently (23) lead to values 3 times lower than the correct average (24).[62] This means that if a localized initial condition lasts long enough for biological purposes when submitted to a Langevin bath (fully classical) it will probably last long enough also when submitted to mixed quantum-classical baths. While this is true, it should be remembered that most localized states are not solitons (in the case of the Davydov model the soliton is just one state while the number of Anderson localized states is infinite) and that measuring average localization does not mean measuring the average stability of the soliton state.

The accuracy of the mixed quantum-classical regime can also be evaluated by comparing its predictions to those of the full quantum regime. This has been done selecting again as variable the lattice displacement correlated with the position of the amide I excitation.[22,42] It was found that, in both regimes, below 10 K, the amide I state induces a localized distortion over typically three sites. At 0.7 K, the mixed quantum-classical average contraction underestimates the full quantum average by approximately 15%, and this difference decreases as temperature increases so that above 10 K the two regimes give virtually the same average lattice contraction, localized on essentially one site.[42]

What can then be said about the thermal stability of the Davydov soliton at equilibrium? A quick calculation is like this. The distortion induced by the amide I excitation when it is localized at single site is χ / κ. This is the maximum distortion that the amide I excitation can induce in the lattice. On the other hand, the thermal fluctuations of a harmonic site are, on average, $\sqrt{k_B T/\kappa}$. When the latter are larger than the former, the displacements induced by thermal noise are larger than those induced by the presence of the excitation and the soliton becomes unstable. Namely, for temperatures for which $\sqrt{k_B T/\kappa} > \chi/\kappa$, that is, for $T > \chi^2/(\kappa k_B)$ the soliton disappears. Using the α-helix values in Table I we conclude that above 21.4 K the Davydov soliton is thermally unstable. However, if its lifetime is sufficiently large, the Davydov soliton may still be of use in biological processes. In the next section the thermal lifetimes of the four states considered in Sec. 6 will be evaluated, using Langevin equations.

7.2. Non-equilibrium

Here we use the approach first applied to the Davydov soliton by Lomdahl and Kerr[21] which consists of adding stochastic forces $F_n(T)$ and damping terms to Eqs. (14) and (15), transforming them into the following Langevin equations:

$$im\frac{d\varphi_n}{d\tau} = (q_{n+1} - q_{n-1})\varphi_n + \nu(\varphi_{n+1} + \varphi_{n-1}), \tag{25}$$

$$\frac{d^2 q_n}{d\tau^2} = (q_{n+1} + q_{n-1} - 2q_n) + (|\varphi_{n+1}|^2 - |\varphi_{n-1}|^2) + F_n(\tau) - \Gamma\frac{dq_n}{d\tau}, \tag{26}$$

where stochastic forces and the friction parameter Γ obey the

fluctuation-dissipation relation: [63]

$$\ll F_n(\tau)F_m(\tau') \gg = 2\Gamma T'\delta_{mn}\delta(\tau - \tau'), \tag{27}$$

where T' is related to the real temperature T by

$$T' = \frac{k_B T}{\chi^2/\kappa} \tag{28}$$

and Γ and the forces $F_n(T)$ are also made non-dimensional by normalization by Ω and χ, respectively. In order to isolate the influence of the parameters v and m, as well as the temperature, all stochastic forces $F_n(T)$ are associated with the same Wiener process, as in Ref. 23.

Fig. 9 shows the dynamics for $T' = 0.05$. Even at this low temperature [equivalent to 1.07 K with the α-helix parameters used in the dynamical Eqs. (25) and (26)] the effect of scattering by thermal phonons on the amide I state is already visible. None of the initial localized states disperses during the time interval simulated, but their trajectories do deviate from the trajectories they have in the absence of the thermal bath (compare with Fig. 5). The lattice distortions correlated with the position of the amide I excitation are more clearly visible when the starting solution is a minimum energy state (two bottom panels), but also they are also apparent for the truncated Gaussian (top right panel). On the other hand, the momenta of the sites are already totally randomized, for all four initial states. Another similarity between the evolution from the four initial states is that, while in Fig. 5 the states did not move now all of them have the same general tendency of moving towards lower n values. This may be due to the fact that the sequence of stochastic forces acting on the lattice sites is the same for all of them, as explained above. In this way, the differences in the evolution can be more clearly attributed to the initial state and to the temperature level.

In Fig. 10 the dimensionless temperature T' is 0.5 and all the other parameters are as for Fig. 9. The physical temperature is now only 10.7 K and all the initial conditions disperse within 10–30 ps. Any correlation between lattice displacements and the amide I excitation is completely buried in the noise.

Considering now the finite temperature equivalent of Fig. 6, for $T' = 0.05$ we have the dynamics displayed in Fig. 11. The slowing down effect of the greater value of m is again clear in all the plots and breather oscillations become visible in the amide I probability distributions, particularly for the two minimum energy states (bottom panels). Also, the correlation between the amide excitation and the induced lattice contraction is clearly seen, for the minimum energy initial conditions and the truncated Gaussian (top right panel). On the contrary, the excitation at a single site splits into two peaks that move in opposite directions each without any visibly associated lattice contraction.

Increasing the temperature to $T' = 0.5$ and keeping everything else as in Fig. 11 we get the dynamics displayed in Fig. 12. Breather oscillations are visible now for the truncated Gaussian and for the minimum energy state at the bottom right panel. The other minimum energy state, at the bottom left, also oscillates but with no apparent frequency. On the other hand, the excitation at a single site still splits into two and the peak that travels to the lower n values disperses at approximately the first third of the time interval. Also, for all four initial conditions, the correlations between the amide I excitation and the lattice displacements have disappeared, so, even if the $|\varphi_n|^2$ plots show the presence of localized solutions, they cannot be considered as arising from the nonlinear interaction between the amide I and the lattice (4). Very frequently such states are nevertheless considered to be solitons but it is more probable that they arise from the disorder in the lattice in which case they should be considered as another example of Anderson localization.

8. EXPERIMENTAL EVIDENCE

While the theoretical feasibility of the Davydov model remains controversial, another possible avenue is to look for experimental evidence. The first apparent experimental evidence for a Davydov-soliton-like state came from the crystal of acetanilide (ACN). This crystal is maintained by hydrogen bonded chains such as (HBC) above and for this reason it can be considered a model for the study of energy transfer in proteins. Careri and co-workers found that when the ACN crystal is cooled a new, so-called anomalous band appears in the amide I region of the absorption spectrum.[32,64] The latter band is 16 cm^{-1} below the conventional band which, in ACN, is centered at 1666 cm^{-1}. The anomalous band was interpreted as due to self-trapped amide I states while the conventional energy band was supposed to be due to exciton states. Later, 2DIR experiments by Hamm and co-workers indicated that while the anomalous peak has an anharmonic behavior, the conventional peak behaves harmonically,[65–67] which seemed to confirm Careri *et al.* interpretations.[32,64] However, those interpretations pose theoretical problems one of which is that purely exciton states are not eigenstates of the Davydov Hamiltonian (1)–(4).[68] Another problem, pointed out by Davydov and already mentioned above, is that a self-trapped state forms by a lattice distortion that is induced by the excitation, and if the associated Franck–Condon factor is too small, the formation of a self-trapped via photon absorption is effectively forbidden.[4,6,40] Following the latter argument, it has been suggested that both absorption lines in the amide I region of crystalline ACN may be due to the amide I states that arise in the different accessible ACN conformations at different temperatures.[69] The idea is that thermal agitation will always distort the hydrogen bonded-chain, but to a greater degree at higher temperatures. If the amide I energy depends not only on the distance between the sites, as proposed in (4), but also on the orientation of hydrogen-bonds, it is possible to obtain two lines in the absorption spectrum, even if the distribution of hydrogen bond lengths has only one peak,[69] as determined experimentally.[70]

The previous paragraph shows that, if the Davydov soliton raises questions that are difficult to settle theoretically, the interpretation of experimental results is also not without its own difficulties. But the experimental measurements raised one more fundamental (and old) question, namely, that of the radiative lifetime of the Davydov soliton. Even if, theoretically, the thermal lifetime of particular Davydov solitons is tens of picoseconds, this is not much use if its life is cut short by radiative means. Recent measurements of the radiative lifetime of amide I excitations lead to values of a few picoseconds in ACN[67] and 20 ps in myosin.[71] Another question is what is the minimum lifetime amide I states

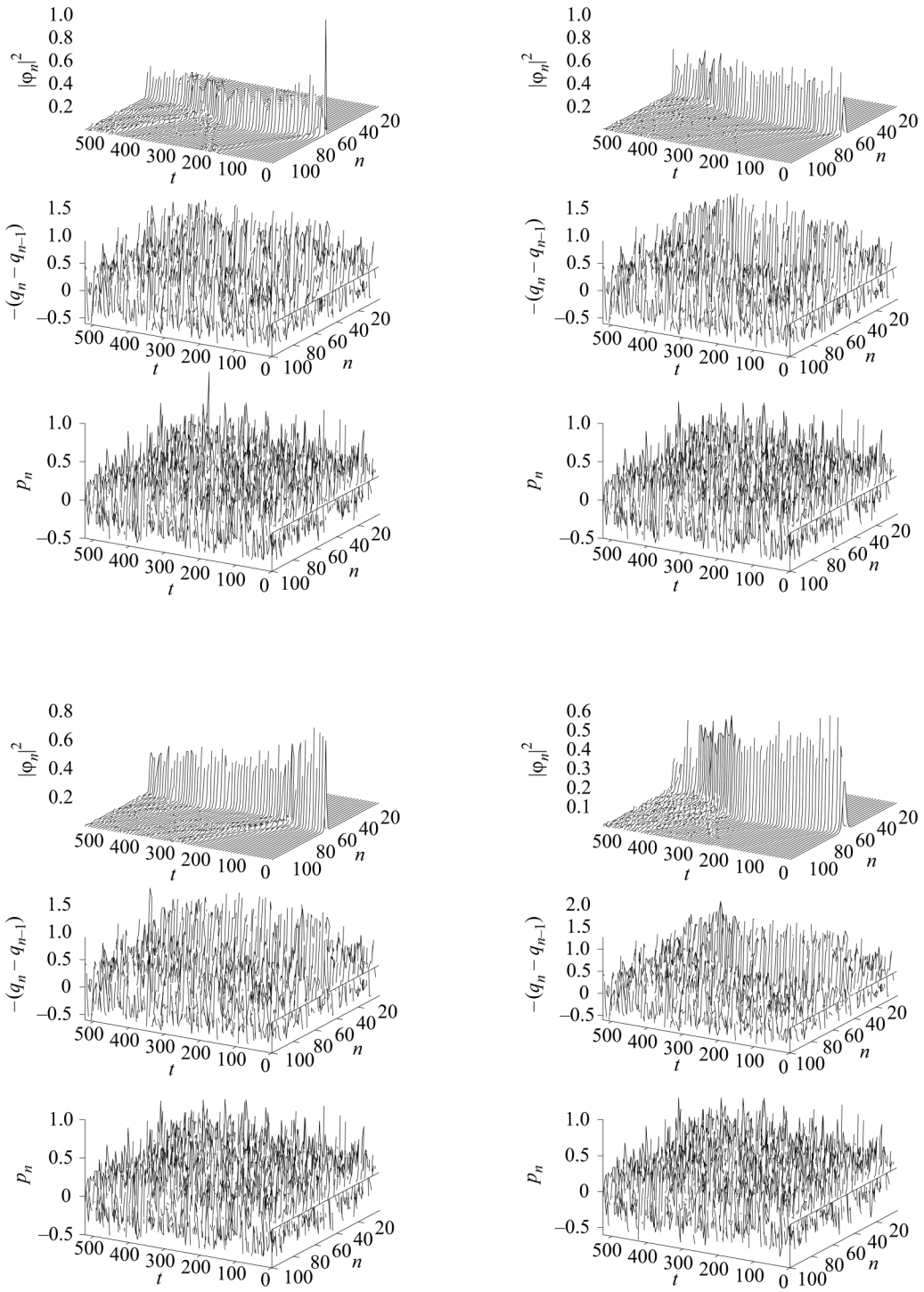

FIG. 9. Dynamical evolution with $v = -0.524$, $m = 2.95$, $T' = 0.05$, and $\Gamma = 0.005$ (see text). Initial conditions are: one site excited at $n = 50$ (top left), truncated Gaussian (top right), minimum energy states for $v = -0.524$ (bottom left) and for $v = -1.645$ (bottom right). Equations (25) and (26) have been used. In each panel the top plot displays the probability amplitude for the amide I excitation to be in lattice site n, $|\varphi_n|^2$, the middle plot displays the local contraction of the lattice $-(q_n - q_{n-1})$, and the lower plot displays the momenta p_n of each lattice site, as function of time.

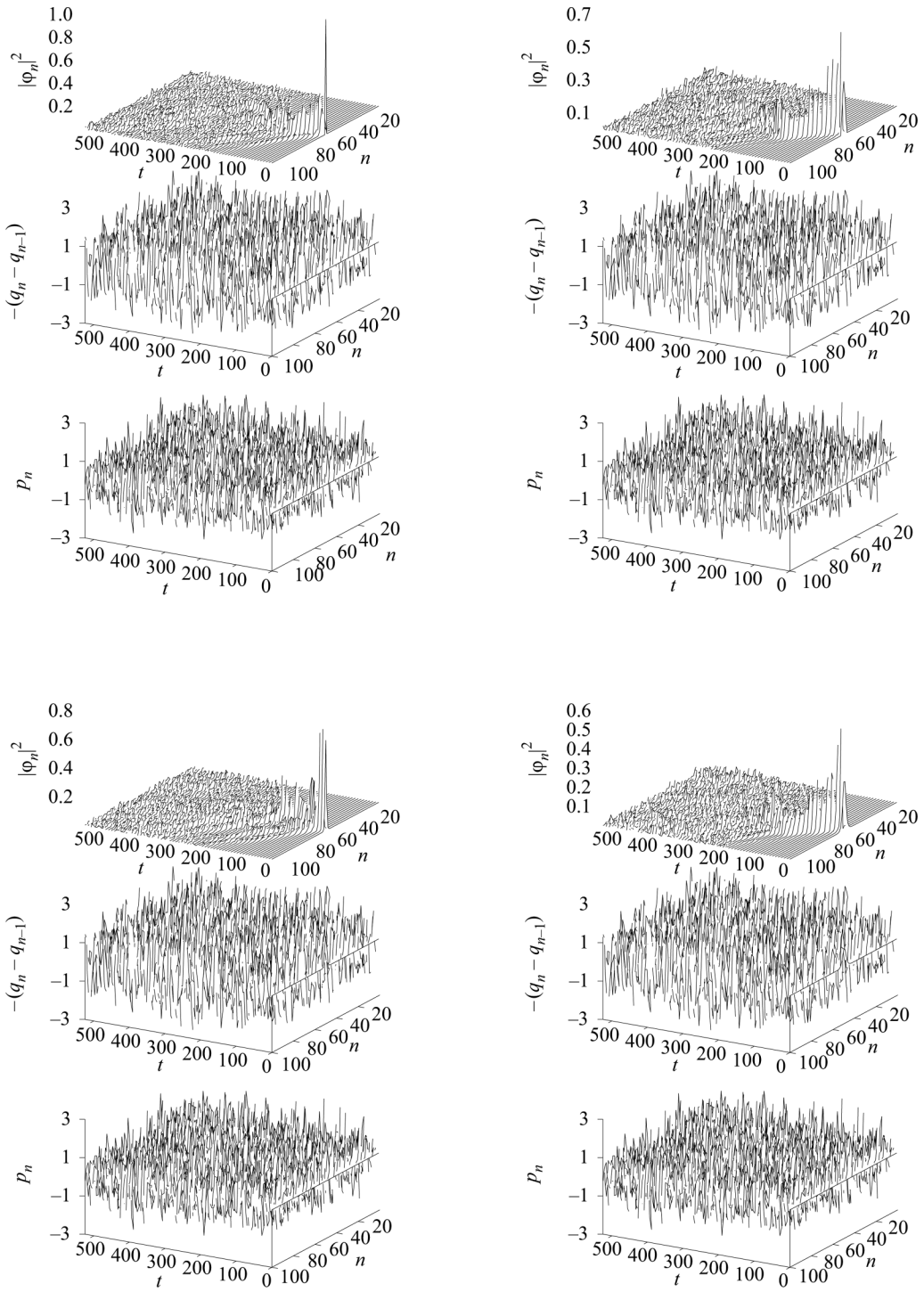

FIG. 10. Dynamical evolution with $v = -0.524$, $m = 2.946$, $T' = 0.5$, and $\Gamma = 0.005$ (see text). Initial conditions are: one site excited at $n = 50$ (top left), truncated Gaussian (top right), minimum energy states for $v = -0.524$ (bottom left) and for $v = -1.645$ (bottom right). Equations (25) and (26) have been used. In each panel the top plot displays the probability amplitude for the amide I excitation to be in lattice site n, $|\varphi_n|^2$, the middle plot displays the local contraction of the lattice $-(q_n - q_{n-1})$, and the lower plot displays the momenta p_n of each lattice site, as function of time.

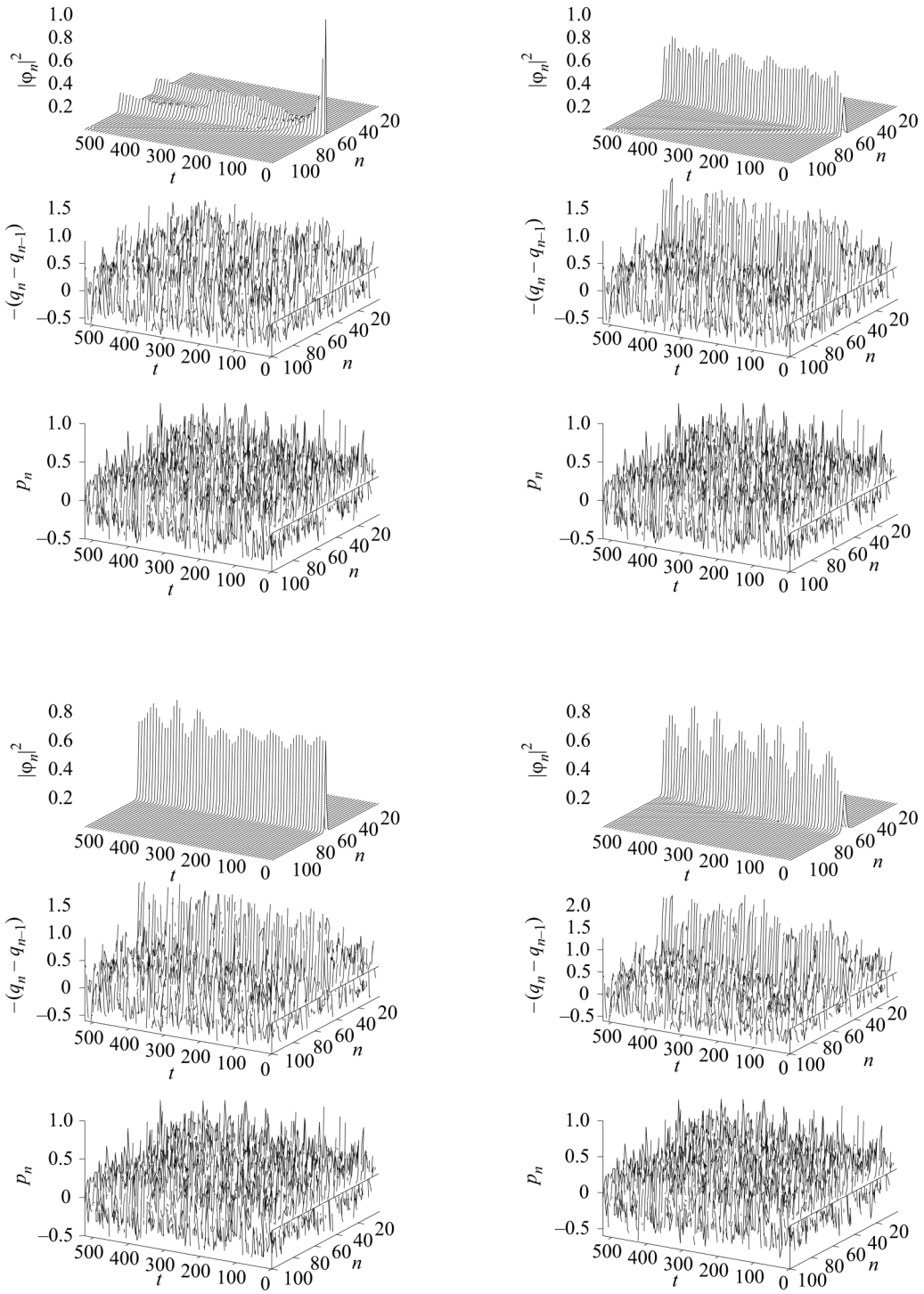

FIG. 11. Dynamical evolution with $v = -0.524$, $m = 9.25$, $T = 0.05$, and $\Gamma = 0.005$ (see text). Initial conditions are: one site excited at $n = 50$ (top left), truncated Gaussian (see text) (top right), minimum energy states for $v = -0.524$ (bottom left) and for $v = -1.645$ (bottom right). Equations (25) and (26) have been used. In each panel the top plot displays the probability amplitude for the amide I excitation to be in lattice site n, $|\varphi_n|^2$, the middle plot displays the local contraction of the lattice $-(q_n - q_{n-1})$, and the lower plot displays the momenta pn of each lattice site, as function of time.

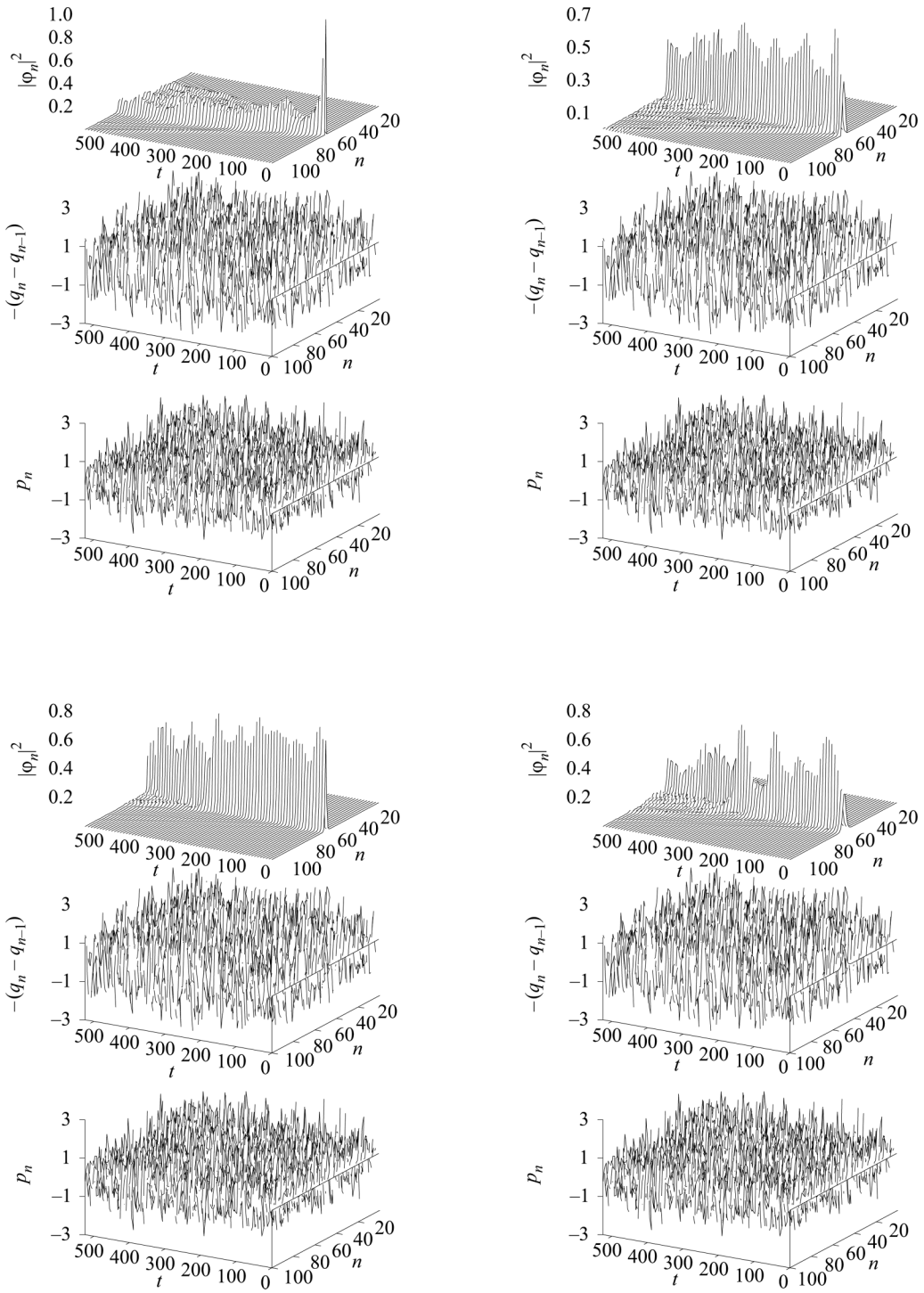

FIG. 12. Dynamical evolution with $v = -0.524$, $m = 9.25$, $T' = 0.5$, and $\Gamma = 0.005$ (see text). Initial conditions are: one site excited at $n = 50$ (top left), truncated Gaussian (see text) (top right), minimum energy states for $v = -0.524$ (bottom left) and for $v = -1.645$ (bottom right). Equations (25) and (26) have been used. In each panel the top plot displays the probability amplitude for the amide I excitation to be in lattice site n, $|\varphi_n|^2$, the middle plot displays the local contraction of the lattice $-(q_n - q_{n-1})$, and the lower plot displays the momenta pn of each lattice site, as function of time.

must have to be useful in biological processes. The answer to this question is also controversial. In Ref. 21 it was suggested that 100–150 ps was not enough, while other authors think that tens of picoseconds,[23] or even just a few picoseconds,[36,72,73] may be sufficient. The latter and much shorter minimum lifetime value is also connected with a view of the role of amide I excitations that is different from that first considered by Davydov, as explained in the next section.

9. THE ROLE OF AMIDE I DECAY

Let us start by distinguishing between energy transfer and energy transduction. While the former refers to the transport of energy from one point to another, the latter refers to the transformation of the energy transported into another form. Davydov aimed at an explanation of muscle contraction[1,8,9] and envisaged the two together: as the soliton transported the amide I energy, it also produced lattice distortions and these transduced part of the energy into the mechanical action of muscle contraction in which myosin molecules would move as a snake, dragging the thin actin filaments as they moved along. As Davydov wrote: "In the theory proposed here (and agreeing with the experimentally established "sliding model") the whole long helical protein molecule (and not only the head section as in Davies' theory) is the working element of the muscle".[1] However, the timescales of soliton propagation, which is of the order of tens of picoseconds and of muscle contraction, which is milliseconds or more, do not fit with Davydov's full model of muscle contraction. Instead, the proposal described in this section is that the role of the Davydov model is to explain energy transfer and that energy transduction is triggered by the decay of the amide I. While in Davydov's theory the energy consumed in muscle contraction is only the kinetic energy of the lattice, according to the latter suggestion the energy stored in the amide I excitation also contributes to the work done.

If the role of the Davydov model is just to describe amide I transfer in proteins, amide I excitations need last only long enough for this vibrational excitation to travel from the active site, where they are created by the hydrolysis of ATP or the binding of ligands, to the sites where their energy is used for work. Conformational changes associated with work occur after the amide I has decayed. In this way, the decay of the amide I is not the end of the process but rather the trigger for the beginning of the transduction of the amide I energy into work.

The feasibility of the ideas put forward in the previous paragraph was tested in the folding of a small protein.[36,73,74] Starting from an initial α-helix, it was shown that using the energy released in amide I decay to impulsively break the hydrogen bond linked to the previously excited C═O group, can lead to the bending of the helix and to the consequent folding of the initial helix into the helical hairpin that constitutes the native state of this protein. This shows that a localized delivery of energy can induce a large scale conformational change in a protein. This is a fundamentally classical process of energy transduction and the proposal here is that it happens after the quantum amide I excitations have decayed.

In this view, the Davydov model explains the transfer of energy from the active site where the energy is generated (by the hydrolysis of ATP or otherwise) to other regions of the protein where the energy is needed for work. This transfer does not need to be coherent it just needs to be non-dissipative. For instance, if it is stochastic, as first envisaged by Holstein,[75] it works just as well. In modeling muscle contraction, Davydov coupled the energy transport to the work, but this is not needed. And also not needed is for the propagation of the energy to be coherent. An incoherent propagation that delivers the energy in full at the right spot is just as good. Probably even more so because it can survive many mutations, as protein work does. And to fulfil the simpler role of transferring energy, amide I vibrations need only last long enough to deliver their energy where it is required. Once gathered at the right place, amide I excitations may decay, in a radiationless manner that releases their energy to the classical degrees of freedom of the protein. The conformational change that takes place after amide I decay can take much longer than the few picoseconds of amide I's lifetime which explains the fact that protein work cycles take so much longer than the time of soliton propagation. In this way, the decay of the amide I vibrations, instead of being a pernicious event that apparently takes place too soon is in fact the trigger without which the dramatic classical events that are observed in relation to many processes in cells would not take place. Amide I propagation may be very short indeed, but it is nevertheless a crucial part of the processes that go on in living cells.

10. DISCUSSION

The Davydov model has been studied by many authors, for several decades and in a great variety of contexts. This work centered on the fully classical and mixed quantum-classical regimes and considered only the essential features of the model in order to put forward a very particular perspective.

The zero temperature studies in Sec. 6 illustrate the rich variety of dynamical behavior that can arise for amide I propagation within the Davydov model, from soliton propagation to different breather solutions and to dispersion.

The problems surrounding the evaluation of the thermal stability of the Davydov soliton were briefly exposed without an attempt to arrive at a definitive answer. On the contrary, the point was to show that due to many uncertainties concerning, for instance, the value of parameters, the nature of the initial condition and of the thermal baths, the level of theory applied, it is impossible to have a theoretical answer about the thermal lifetime of the Davydov soliton. And perhaps a deeper problem than evaluating the lifetime is to understand how a state as regular as a soliton can appear in systems as structurally and dynamically irregular as proteins.

According to the proposal in Sec. 9 it is not important for the amide I states to be solitons and for the transfer to be coherent. The calculations show that many types of localized states arise at finite temperature, not because of the nonlinear interaction which certainly exists between the amide I and amide group displacements, but, most probably because of disorder in the chain, i.e., of Anderson localization.

Furthermore, it was suggested that more limiting than the thermal lifetime is the problem of the radiative lifetime of the amide I, a problem that brings this field back to the starting point. How can we escape this circle? One solution, as proposed in the previous section, is to assume that amide I excitations are simply carriers of energy and that energy transduction (the work done

TABLE II. Table of knowns and unknowns in the Davydov model .

	Classical	Mixed quantum-classical	Quantum Mechanical
$T = 0$ K	Exactly solvable numerically	Exactly solvable (=classical)	Exactly solvable analytically for $V = 0$, numerically for the dimer
$T > 0$ K (Equilibrium)	Exact numerical solution	Exact numerical solution	Exact numerical solution
$T > 0$ K (Non-equilibrium)	Langevin Eqs. valid	?	?

with the energy they carry) is performed after they have decayed and released their internal energy for the necessary work. In this way, even a radiative lifetime of a few picoseconds may be enough for the Davydov model to be useful for biological work.

11. CONCLUSION

Table II is a tentative summary of the theoretical knowns and unknowns about the Davydov model, distinguishing between the three main regimes: fully classical in which both the lattice site motions and the amide I vibration are treated classically, mixed quantum-classical, in which the lattice site motions are classical but the amide I vibration is treated quantum mechanically and fully quantum in which both the lattice and the amide I are treated quantum mechanically.

In Sec. 3 it was pointed out that the equations of motion obtained from the so-called D_2 ansatz, which start from the fully quantum regime, are in fact equivalent to those obtained from an exact derivation within the mixed quantum-classical regime. For $T = 0$ K the equations of motion are exactly solvable numerically for the mixed quantum-classical which is then equivalent to the fully classical regime.

For $T > 0$ K two cases are considered: the equilibrium state and non-equilibrium. As discussed in Ref. 35 the equilibrium properties can be obtained by Monte Carlo methods in all regimes and simulations have shown that, with the parameter values used here, above 10 K the lattice contraction correlated with the position of the amide I vibration is approximately equal in the mixed quantum-classical and fully quantum regimes[42] and much larger than that obtained in the fully classical regime.[35]

In the non-equilibrium regime, only the fully classical regime can be simulated exactly,[63] for instance, via Langevin equations. Numerical methods for finite-temperature non-equilibrium simulations of mixed quantum-classical and fully quantum regimes have been devised,[35,43,76,77] but their validity has yet to be proven.

Finally, it should be noted, however, that these considerations relate to a proof of principle, i.e., a proof of the theoretical viability of the Davydov model. Even if such a proof is eventually found, it still leaves out the great unknown, namely, to determine whether the Davydov mechanism is in fact used by living cells. That kind of proof can only come from experiments.

ACKNOWLEDGMENTS

L.C. acknowledges Portuguese national funds from FCT—Foundation for Science and Technology through projects UIDB/04326/2020, UIDP/04326/2020 and LA/P/0101/2020.

REFERENCES

[1] A. S. Davydov, J. Theor. Biol. **38**, 559 (1973).
[2] A. S. Davydov and N. I. Kislukha, Phys. Status Solidi B **59**, 465 (1973).
[3] A. S. Davydov and N. I. Kislukha, Phys. Status Solidi B **75**, 735 (1976).
[4] A. S. Davydov, J. Theor. Biol. **66**, 377 (1977).
[5] A. S. Davydov, Phys. Scr. **20**, 387 (1979).
[6] A. S. Davydov, Int. J. Quant. Chem. **16**, 5 (1979).
[7] A. S. Davydov, Physica D **3**, 1 (1981).
[8] A. S. Davydov, *Biology and Quantum Mechanics* (Pergamon Press, Oxford–Frankfurt, 1982).
[9] A. S. Davydov, Sov. Phys. Usp. **25**, 898 (1982).
[10] A. S. Davydov, Phys. Status Solidi B **138**, 559 (1986).
[11] C. W. F. McClare, Ann. N. Y. Acad. Sci. **227**, 74 (1974).
[12] S. Krimm and J. Bandekar, Adv. Prot. Chem. **38**, 181 (1986).
[13] J. M. Hyman, D. W. McLaughlin, and A. C. Scott, Physica D **3**, 23 (1981).
[14] A. C. Scott, Phys. Scr. **25**, 651 (1982).
[15] A. C. Scott, Phys. Rev. A **26**, 578 (1982).
[16] A. C. Scott, Phys. Lett. A **94**, 193 (1983).
[17] A. C. Scott, Phys. Scr. **29**, 279 (1984).
[18] L. Macneil and A. C. Scott, Phys. Scr. **29**, 284 (1984).
[19] A. C. Scott, Phil. Trans. R. Soc. A **315**, 423 (1985).
[20] A. Scott, Phys. Rep. **217**, 1 (1992).
[21] P. S. Lomdahl and W. C. Kerr, Phys. Rev. Lett. **55**, 1235 (1985).
[22] X. Wang, D. W. Brown, and K. Lindenberg, Phys. Rev. Lett. **62**, 1796 (1989).
[23] D. D. Georgiev and J. F. Glazebrook, Chaos Solit. Fractals **155**, 111644 (2022).
[24] J. C. Eilbeck, P. S. Lomdahl, and A. C. Scott, Phys. Rev. B **30**, 4703 (1984).
[25] L. Cruzeiro, J. Phys. Condens. Matter. **17**, 7833 (2005).
[26] N. A. Nevskaya and Y. N. Chirgadze, Biopolymers **15**, 637 (1976).
[27] V. A. Kuprievich and Z. G. Kudritskaya, *Technical Report* (Institute for Theoretical Physics, Kyiv, Ukraine, 1982).
[28] K. Itoh and T. Shimanouchi, Adv. Prot. Chem. **38**, 181 (1986).
[29] V. A. Kuprievich, in *Davydov's soliton revisited self-trapp-ing of vibrational energy in protein*, edited by P. L. Christiansen and A. C. Scott, NATO Sci. Peace Secur. B Phys. Biophys. **243**, 199 (1990).
[30] B. M. Pierce, in *Davydov's soliton revisited self-trapping of vibrational energy in protein*, edited by P. L. Christiansen and A. C. Scott, NATO Sci. Peace Secur. B Phys. Biophys. **243**, 209 (1990).
[31] N. Ostergaard, in *Davydov's soliton revisited self-trapping of vibrational energy in protein*, edited by P. L. Christiansen and A. C. Scott, NATO Sci. Peace Secur. B Phys. Biophys. **243**, 229 (1990).
[32] G. Careri, U. Buontempo, F. Galluzzi, A. C. Scott, E. Gratton, and E. Shyamsunder, Phys. Rev. B **30**, 4689 (1984).
[33] Y. Zhao, K. Sun, L. Chen, and M. Gelin, WIREs Comput. Mol. Sci. **12**, e1589 (2022).
[34] W. C. Kerr and P. S. Lomdahl, Phys. Rev. B **35**, 3629 (1987).
[35] L. Cruzeiro-Hansson and S. Takeno, Phys. Rev. E **56**, 894 (1997).
[36] L. Cruzeiro, Z. Phys. Chem. **230**, 743 (2016).
[37] M. Springborg, *Methods of Electronic-Structure Calculations. From Molecules to Solids* (John Wiley & Sons, Chichester–Toronto, 2000).
[38] L. A. Cisneros-Ake, L. Cruzeiro, and M. G. Velarde, Physica D **306**, 82 (2015).

[39]A. S. Davydov and A. A. Eremko, Ukr. Fiz. Zh. **22**, 1088 (1977).
[40]A. S. Davydov, *Solitons in Molecular Systems*, (Reidel, Dord-recht, 1991).
[41]L. Cruzeiro-Hansson, Physica D **68**, 65 (1993).
[42]L. Cruzeiro-Hansson and V. M. Kenkre, Phys. Lett. A **203**, 362 (1995).
[43]J. Cuevas, P. A. S. Silva, F. R. Romero, and L. Cruzeiro, Phys. Rev. E **76**, 011907 (2007).
[44]L. S. Brizhik and A. S. Davydov, Phys. Status Solidi B **115**, 615 (1983).
[45]D. Emin and T. Holstein, Phys. Rev. Lett. **36**, 323 (1976).
[46]G. Venzl and S. F. Fischer, J. Chem. Phys. **81**, 6090 (1984).
[47]P. Nagy, J. Phys. C **20**, 5527 (1987).
[48]M. Wagner and A. Köngeter, Phys. Rev. B **39**, 4644 (1989).
[49]L. Cruzeiro-Hansson and V. M. Kenkre, Phys. Lett. A **190**, 59 (1994).
[50]V. M. Kenkre, *Interplay of Quantum Mechanics and Non-Linearity: Understanding Small-System Dynamics of the Discrete Nonlinear Schroedinger Equation* (Springer, Cham, Switzerland, 2022).
[51]A. A. Eremko, in *Davydov's soliton revisited self-trapping of vibrational energy in protein*, edited by P. L. Christiansen and A. C. Scott, NATO Sci. Peace Secur. B Phys. Biophys. **243**, 429 (1990).
[52]L. Brizhik, L. Cruzeiro-Hansson, and A. Eremko, J. Biol. Phys. **24**, 19 (1998).
[53]L. Brizhik, L. Cruzeiro-Hansson, and A. Eremko, J. Biol. Phys. **24**, 223 (1999).
[54]L. Brizhik, Electromagn. Biol. Med. **34**, 123 (2015).
[55]G. Careri and J. Wyman, Proc. Natl. Acad. Sci. USA **81**, 4386 (1984).
[56]S. Aubry, Physica D **216**, 1 (2006).
[57]S. Flach, and A. V. Gorbach, Phys. Rep. **467**, 1 (2008).
[58]A. S. Davydov, Sov. Phys. JETP **51**, 397 (1980).
[59]A. S. Davydov, in *Davydov's Soliton Revisited. Self-Trapping of Vibrational Energy in Protein*, NATO ASI Series, Series B: Physics, edited by P. L. Christiansen and A. C. Scott, (Plenum Press, New York, 1990), Vol. 243.
[60]A. S. Davydov, J. Phys. I **1**, 1649 (1991).
[61]L. Cruzeiro-Hansson, Phys. Rev. A **45**, 4111 (1992).
[62]L. Cruzeiro-Hansson, Phys. Rev. Lett. **73**, 2927 (1994).
[63]R. Kubo, Rep. Progr, Phys. **29**, 255 (1966).
[64]G. Careri, U. Buontempo, F. Carta, E. Gratton, and A. C. Scott, Phys. Rev. Lett. **51**, 304 (1983).
[65]J. Edler, P. Hamm, and A. C. Scott, Phys. Rev. Lett. **88**, 067403 (2002).
[66]J. Edler and P. Hamm, J. Chem. Phys. **117**, 2415 (2002).
[67]J. Edler and P. Hamm, J. Chem. Phys. **119**, 2709 (2003).
[68]P. Hamm and G. P. Tsironis, Eur. Phys. J. Special Topics **147**, 303 (2007).
[69]L. Cruzeiro, in *Quodons In mica nonlinear localized Tra-velling excitations in crystals*, edited by J. F. R. Archilla, N. Jimenez, V. J. Sanchez-Morcillo, and L. M. Garcia-Raff (Springer Series in Materials Science. 2015), Vol. **221**, p. 401.
[70]S. W. Johnson, J. Eckert, M. Barthes, R. K. McMullan, and M. Muller, J. Phys. Chem. **99**, 16253 (1995).
[71]R. H. Austin, A. H. Xie, L. van der Meer, B. Redlich, and H. P. A. Lindgard, Phys. Rev. Lett. **94**, 128101 (2005).
[72]L. Cruzeiro, DCDS **4**, 1033 (2011).
[73]L. Cruzeiro, Pure Appl. Chem. **92**, 179 (2020).
[74]L. Cruzeiro, in *Nonlinear systems*, edited by J. Archilla, F. Palmero, M. Lemos, B. Sánchez-Rey, and J. Casado-Pascual, *Understanding Complex Systems*, (Springer, Cham, 2018), Vol. 2, p. 3.
[75]T. Holstein, Ann. Phys. **8**, 343 (1959).
[76]L. Cruzeiro-Hansson, Europhys. Lett. **33**, 655 (1996).
[77]L. Cruzeiro-Hansson, Phys. Lett. A **223**, 383 (1996).